Colloidal Allostery

Exploring the pathway to innovative separation technology

Yug Chandra Saraswat

Technische Universiteit Delft

TU Delft Delft University of Technology

Challenge the future

Colloidal Allostery

Exploring the pathway to innovative separation technology

by

Yug Chandra Saraswat

in partial fulfillment of the requirements for the degree of

Master of Science
in Chemical Engineering (Process Track)

at the Delft University of Technology,
to be defended publicly on Friday May 18, 2018 at 10:00 AM.

Supervisor:	Dr. H. B. Eral	
Thesis committee:	Prof. dr. J. H. van Esch,	TU Delft
	Dr. H. B. Eral,	TU Delft
	Dr. O. Moultos,	TU Delft

TU Delft Delft University of Technology

Preface

Colloidal allostery is a regulatory mechanism where specific metabolites regulate the protein activity by binding to them and changing their energy landscape. The first steps to model this system on a colloidal scale were made by studying the depletion interaction between the hydrogel posts and the rigid polystyrene particles. Using soft lithography, hydrogel posts of different rigidity were synthesized inside the microfluidic channel. Polystyrene particles and depletant (dextran) were added and the interaction between the posts and the particles was studied using optical microscopy and particle tracking.

However, major issues such as poor statistics, incomplete cross-linking of the hydrogel posts and irreversible sticking of polystyrene particles to the hydrogel hindered with the experimental results. Therefore, in this project, efforts are made to improve the experimental implementation of the model.

At the end of the project, it was observed that while optical tweezers offer a more controlled and refined way of measuring the interactive forces than the particle tracking using video microscopy, the limitations of the equipment in providing the location of the particle normal to the base of the channel hinder the estimation of the desired parameter. Furthermore, despite curing the hydrogel posts for a long period of time under the UV light, the rigid polystyrene particles still stick irreversibly to the post.

It is therefore recommended that the optical tweezer apparatus must be upgraded to provide the researcher with the position of particle normal to channel bottom. This can allow better estimation of the effect of the wall on the motion of the particle. The photo-crosslinking characteristics of the hydrogel must be studied to determine the effect of the UV light on the gelation process.

The ultimate vision of the project is to develop innovative separation technologies based on the fundamental understanding of the interplay of the depletion forces and elastic energy of deformation of the hydrogel posts.

Yug Chandra Saraswat
Delft, May 2018

Contents

1

Introduction

Allostery, deemed to be the "second secret to life", next only to the genetic code [1] by Jacques Monod, is a term used to describe the regulation of biological proteins by specific metabolites that alter the conformation of the protein when they bind to it [2]. Hemoglobin shows a special kind of allosteric mechanism whereby the binding of a single oxygen molecule alters the energy landscape of the protein to ease the binding of another oxygen molecule. Similarly, the unbinding of oxygen from the protein alters the energy landscape to facilitate easy unbinding of other oxygen molecule. This is also termed as the cooperative effect [3].

This process of reversible binding of a substrate molecule to a protein served as the original inspiration for this project. The process of reversible binding is intended to be understood on a colloidal scale through a simple model consisting of a force that drives the substrate to bind to the wall (called the depletion force) and an opposing force that controls the deformation of the wall upon contact (called the deformation force). The interplay of these 2 forces results in an energy potential well. By manipulating the depth of this energy well, which is a function of the strength of attractive force and the opposing force, it is possible to control the tendency of the substrate to bind to the wall.

On the colloidal scale, the tendency of the substrate to bind to the post is a function of the strength of the depletion force and the unbinding of the substrate from the wall is proposed to be the function of the wall's elasticity. Elasticity can be defined as the property of a material that characterizes the ease with which the material can be deformed.

In this project, polyethyleneglycol diacylate (PEGDA) cylindrical hydrogel pillars (called posts) made inside a microfluidic channel serve as deformable walls and polystyrene (PS) particles serve as rigid spherical substrates. The elasticity of the hydrogels can be tuned based on the molecular weight of the PEGDA polymer. So, PEGDA 700 is used to make hard posts (with lesser tendency to deform upon contact) and PEGDA 6000 is used to make soft posts (with higher tendency to deform upon contact). The contact of PS spheres with hard post and soft posts should result in energy wells that are distinguishable by the depth of the well.

While the project is not motivated to understand the biological aspects of protein regulation, the vision of the project is to develop innovative separation filters using materials whose elasticity is sensitive to external factors such as the ultraviolet (UV) light or temperature. The elasticity of the filter can be tuned to facilitate the binding of particles or release of the stuck particles.

In the previous work [4], first step was taken to develop a model towards this vision. It was hypothesized that by tracking the motion of the PS particles - moving towards the post, binding reversibly to the post, and moving away from the post - trajectories could be created that would allow the measurement of the time the particle require to escape a potential energy well.

However,issues were faced during the implementation of the proposed model in an experimental set up.

- The PS particles irreversibly stuck to the hydrogel posts resulting in trajectories that could not be used to estimate the escape time. It was hypothesized that this irreversible binding was due to the unspecified interactions between the PS particles and the dangling free chains

of an incompletely cross-linked hydrogel. It was recommended that by curing the hydrogel posts under UV light for a long period of time, complete cross-linking would be achieved. This would, hence, eliminate any dangling free chains and prevent irreversible binding of PS particles to the post.

- The previous depletion experiments based on tracking colloidal particles using video microscopy showed that in the time lapse of an hour less than 5 events of particles reversibly binding to the post were observed. Hence, it was suggested that the technique of generating potential well must be modified to improve the statistics.
- The 3D nature of the microfluidic channel caused the particles to not only enter the plane of focus (during the tracking step) but also diffuse out of the plane of focus. This resulted in particle trajectories that underestimated the escape time. This issue was also considered to be of high importance recommended to be solved should the research is continued.

In this project, the goal was to make efforts to take into account all the issues stated above and modify the experimental methodology to improve the same. Therefore,

- The hydrogel posts, once created were cured under the UV light for a period of 1.5 hours to ensure complete cross-linking.
- Optical tweezers were used to measure the forces experienced by the particle as it is moved closer to the hydrogel post with the intention to develop reliable potential energy against displacement curves and obtain precise estimates of the esacpe time.

This thesis has been primarily structured into 3 chapters. Each chapter is sub-divided into 3 sections.

- Theory - This section covers the underlying theory behind each experiment.
- Experiment - This section covers in detail the experimental methodology, procedure for preparation of samples, precautions to be taken while performing the experiment.
- Results and discussion - This final section summarizes the results obtained from the experiment, issues faced during the experiment and steps taken to deal with those issues

Chapter 2 describes the technique of microrheology. The purpose of this chapter is to introduce the reader to the concepts of particle tracking using softwares such as MATLAB and very useful algorithms behind the MATLAB code developed by John Crocker and David Grier [5]. The particle tracking experiments were originally performed with the intention to apply the tracking technique and trajectory analysis methods towards estimation of parameters (Diffusion coefficient and escape time) in depletion experiments using video microscopy. But, over the course of time it was realized that depletion experiments using optical tweezers would be more effective given the poor statistical results using the former method [4]. Hence, no results for depletion experiments using video microscopy (escape time) have been included in the report. However, estimation of macroscopic properties, such as the diffusion coefficient of particles in aqueous medium, by analyzing particle trajectories have been included.

Chapter 3 describes the theoretical model proposed to understand allosteric mechanism on a colloidal scale. The chapter introduces the reader to the concept of depletion interaction, microstructure of hydrogels, energy required to deform a hydrogel post, energy potential well and finally the escape time. This chapter is important to understand the base of this thesis. Furthermore, it describes the experimental methodology behind the microfluidic channel preparation using lithographic technique, the hydrogel post preparation using photo-crosslinking and the preparation of depletion mixture.

Chapter 4 describes the use of optical trapping technique to measure the forces of interaction between colloidal particles and the hydrogel posts. This chapter provides a brief introduction to the guiding principle behind optical trapping, how the tweezer system is calibrated and how to analyze the errors associated with the measured forces. The chapter is concluded with the analysis of the

force-displacement curves obtained during the control and depletion experiments.

This report ends with chapter 5 on the conclusions based on the results obtained and recommendations to further improve this study. The appendix serves to enhance the reader's understanding of how certain mathematical relations have been derived.

2

Microrheology

Microrheology [6] can be described as a technique useful to extract the local and bulk mechanical properties of a fluid by tracking the motion of microscopic particles suspended in it. In this chapter, we extract the diffusion coefficient of the colloidal particles (ϕ 0.22μm, ϕ 1.337μm, ϕ 1.89μm). The diffusion coefficient of the colloidal particles is estimated from the slope of a linear fit on mean squared displacement (MSD) against lag time (τ) curve. The diffusion coefficient of the colloidal particles can also be estimated from the variance of the distribution fitted over the histogram of particle displacements.

In this chapter, the basic steps involved in particle tracking are enumerated in section 2.1.1 along with the description of particle tracking code developed by Eric Furst [7] based on the algorithms developed by John Crocker and David Grier [5]. The analysis of the particle trajectory to estimate MSD and theory behind the estimation of diffusion coefficient using linear fit on MSD vs τ curve is discussed in section 2.1.2. The chapter also discusses the possible errors that might occur during particle tracking (drift, static error) and trajectory analysis (uncertainty due to fitting) in section 2.1.3

2.1. Theory

2.1.1. Steps in particle tracking

The basic procedure that is followed to track particles include:-

1. Preparation of the sample containing the fluorescent particles of specific size (ϕ 0.22 μm, ϕ 1.337 μm, ϕ 1.89 μm) dispersed in an aqueous medium.

2. Arranging the sample on the stage of the Nikon T*i*-E microscope and observing the particles.

3. Acquiring a video (ND acquisition) of particles in motion, at desired frame rate (40 fps) and exposure time (0.025 s), using the camera integrated into the system.

4. Splitting the acquired video into images (.nd2 extension) using the NIS-Elements viewer 4.20 separated at constant time intervals.

5. Processing the images to create particle trajectories and extract required information (diffusion coefficient of the particles in water)

The images acquired from the above procedure must be processed before tracking particles. Figure 2.1 shows the colloidal particle under EPI mode. The basic steps involved in processing of images are:-

1. Image Filtering and Contrast Adjustment

2. Locating the particles in an image

3. Identifying same particles in all images

4. Creating trajectories

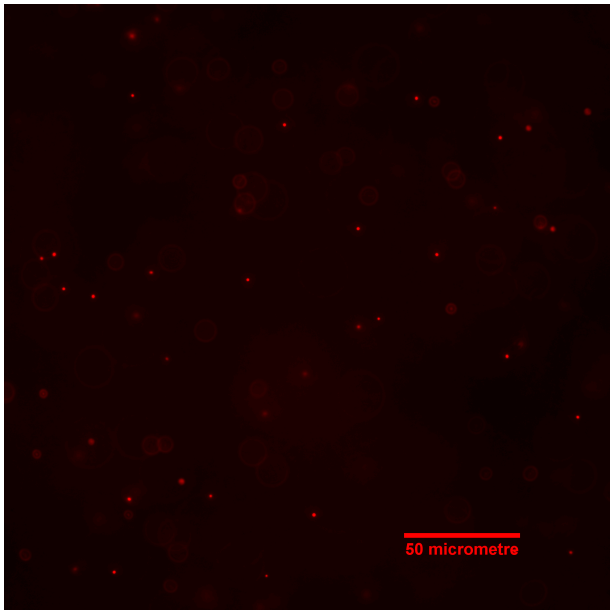

Figure 2.1: Colloidal particles viewed under microscope using EPI mode

Image Filtering

The images acquired from the camera may contain noise due to differences in the contrast over different regions of the image. This can complicate the process of locating particles in the image. Hence, boxcar averaging technique was used to remove the noise due to such gradients and enhance the Signal-to-Noise ratio (SNR) [8].

However, these variations can be removed using a boxcar average [5]. This technique replaces a group of consecutive data points (having coordinates x,y) with their average over a region of $2w+1$, where w is an integer greater than the mean diameter of particles (in pixels), with their average. The improvement in the quality of the signal is proportional to the number of data points taken in the boxcar average. Each pixel is given a new value by

$$I_w(x,y) = \frac{1}{(2w+1)^2} \sum_{i,j=w}^{w} I(x+i, y+j) \tag{2.1}$$

In addition to the noise due to the contrast gradients, each image may also contain some random noise due to camera. Hence, Gaussian filtering technique was used to remove this noise over the same region w. This filter averages the noise value in the nearby pixels with half-width $\xi = 1$ pixel using

$$I_\xi(x,y) = \frac{\sum_{i,j=-w}^{w} I(x+i, y+j) \exp(\frac{-i^2+j^2}{4\xi^2})}{\sum_{i=-w}^{w} \exp(\frac{-i^2}{4\xi^2})} \tag{2.2}$$

Both the noise reduction filters are implemented using MATLAB by Eric et.al.[7]. In addition to the above filters, the Nikon T*i*-E microscope software allows the user to improve the contrast of the image manually and fix the desired contrast settings based on visual inspection.

Locating Particles

The location of particles is calculated based on the brightest pixels [5]. If $I(x,y)$ represents the intensity of particle image then the locally brightest pixels would be those with the highest values within the region of $2w$ pixels (this distance should be less than the average distance between 2 particles). These brightest pixels are close to the center of the image of the particle. A particle

image can be expressed as a 2-D Gaussian centered at the position r_i,

$$I_i(r_i) = I_0 \exp(\frac{-|r - r_i|^2}{s^2}) \tag{2.3}$$

where,
I_i - Intensity of image I_i of the i^{th} particle
The procedure to obtain the raw location of the particles is implemented in MATLAB by Eric et.al. [7].

One thing that has to be kept in mind is that the brightest pixel is not exactly at the center of the fitted Gaussian distribution [5]. Hence, the raw location of the particle must be refined to achieve sub-pixel resolution. For each particle, the intensity weighted centroid served as the refining parameter. The correction was calculated using

$$\begin{pmatrix} \varepsilon_x \\ \varepsilon_y \end{pmatrix} = \frac{1}{m_0} \sum_{i^2+j^2 \le w^2} \begin{pmatrix} i \\ j \end{pmatrix} I(x_0 + i, y_0 + j) \tag{2.4}$$

where,
m_0 (= $\sum_{i^2+j^2 \le w^2} I(x_0 + i, y_0 + j)$) - Integrated brightness of the particle image
The new location estimates of the centroid are given by

$$(x_i, y_i) = (x_0 + \varepsilon_x, y_0 + \varepsilon_y) \tag{2.5}$$

This centroid weighted improvement is implemented using MATLAB by Eric et.al [7].

Identifying same particles in all images

Once the location of all the particles in an image was estimated, identifying the same particle in consecutive images was required to create trajectories of multiple particles as a function of time. A cautious approach must be followed since particles are unconstrained and therefore, have a tendency to move in and out of the focal plane. This will consequently result in different number of particles in different images.

The identification of same particle in consecutive images is done by estimating the maximum distance that a particle can move during a unit time interval. This estimate is based on the assumption that the motion of particles in the sample follows random thermal motion of non-interacting particles. Such an assumption can be considered valid as long as particles are tracked at least 20-25 particle diameters away from the top and bottom glass edges and a dilute aqueous suspension of particles is used as the sample. Both these requirements are fulfilled during the experiment.

The probability that a particle would diffuse over a distance δ in time τ is $P(\delta|\tau)$, given by [9]

$$P(\delta|\tau) = \left(\frac{1}{4\pi D\tau}\right) \exp\left(-\frac{\delta^2}{4D\tau}\right) \tag{2.6}$$

where, D is particle's self diffusion coefficient.
For an ensemble of N non-interacting particles, this probability distribution is modified to

$$P(\delta_i|\tau) = \left(\frac{1}{4\pi D\tau}\right)^N \exp\left(-\sum_{i=1}^{N} \frac{\delta_i^2}{4D\tau}\right) \tag{2.7}$$

The most likely estimate of the position of one particle between 2 consecutive images is the one that maximizes $P(\delta_i|\tau)$ [5].

Creating particle trajectories

The movement of particles in and out of the focal plane has important implications on the creation of particle trajectories. When a particle moves out of the focal plane but returns some time

later, it would be treated as a separate particle and provided with a new identifier. This results in multiple short trajectories which has a negative impact on statistics at longer lag times. Such a problem is most commonly observed with particles smaller than 0.5 μm because the particle mobility is high. However, for larger particle (> 2 μm) with low mobility, this is not a big issue.

Hence, a parameter "memory" is provided in the tracking code [7] to retain the identifier of the particle that briefly moved out of the focal plane. This improves the statistics at longer lag times. Furthermore, parameter "goodenough" is provided to only consider trajectories of specific length for further analysis and eliminate trivial short trajectories (containing only single position) which are of no significance and may act as noise.

2.1.2. Trajectory Analysis

Once the particle positions are concatenated into trajectories, the mean squared displacement (MSD) of the particles is calculated as a function of lag time. MSD is defined as the average squared distance a particle covers within a given time interval (τ), known as lag time [10].
The general formula for particle displacement is

$$\Delta r_{ij} = (\Delta x_{ij} = x_{i(j+\tau)} - x_{ij}, \Delta y_{ij} = y_{i(j+\tau)} - y_{ij}) \tag{2.8}$$

and the formula for mean squared displacement is

$$\Delta\overline{r^2} = \frac{\Delta\overline{x_{ij}^2} + \Delta\overline{y_{ij}^2}}{N_{disp}} \tag{2.9}$$

where,
N_{disp} - Number of displacements for a given lag time

This formula holds as long as the trajectory contains time j and $j+\tau$. In order to understand how MSD is calculated, let us consider an example.

The calculation of MSD requires splitting a particle trajectory i (which last from time j = 0 to j = 3 s) into displacements. So, for a unit lag time,

$$\Delta r_{10} = (\Delta x_{10} = x_{11} - x_{10}, \Delta y_{10} = y_{11} - y_{10})$$
$$\Delta r_{12} = (\Delta x_{12} = x_{12} - x_{11}, \Delta y_{12} = y_{12} - y_{11})$$
$$\Delta r_{13} = (\Delta x_{13} = x_{13} - x_{12}, \Delta y_{13} = y_{13} - y_{12})$$

Similarly, for a lag time of 2 s,

$$\Delta r_{20} = (\Delta x_{20} = x_2 - x_0, \Delta y_{20} = y_2 - y_0)$$
$$\Delta r_{31} = (\Delta x_{31} = x_3 - x_1, \Delta y_{31} = y_3 - y_1)$$

Such calculations can be performed for all trajectories of different lengths at all lag times. Hence, for a given lag time, we obtain a list of displacements from different trajectories. The longer the trajectory and smaller the value of τ, greater will be the number of displacements that can be extracted from the trajectory. This results in a more statistically precise estimation of MSD using equation 2.9.

Diffusion coefficient: Linear fit of MSD vs Lag time

The calculation of MSD includes a time average, since displacements were created at different time points along a trajectory, and an ensemble average, since the displacements come form different particle trajectories. as indicated in 2.9. This MSD is calculated initially, in $pixel^2$ for different lag times (in $frames$). These results must be converted to proper units, i.e. displacement (in μm^2)

as a function of lag time (in s), by using the selected frame rate (in fps) for conversion.
The trajectory of a particle undergoing brownian motion is related to its self diffusion coefficient using the Einstein-Smoluchowsky equation [11].

$$\langle(|r(t+\tau)) - r(t)|)^2\rangle = 2dD\tau \tag{2.10}$$

where,
d - number of dimensions in the trajectory data
The calibrated MSD vs lag time data is, therefore, plotted on a log-log plot and a simple linear regression analysis, using the least squares method, is performed. The general equation for linear curve fitting is [12]

$$y = b_0 + b_1 x \tag{2.11}$$

where,

$$b_0 = \sum_{i=1}^{n} \frac{(x_i - \bar{x})(y_i - \bar{y})}{(x_i - \bar{x})^2} \tag{2.12}$$

The regression equation is slightly modified to force the intercept (b_0) to zero.
The slope of the fitted curve is used to estimate the diffusion coefficient using the following equation

$$\frac{\Delta MSD}{\Delta\tau} = 4D\tau \tag{2.13}$$

The constant 4 (= 2d) in equation 2.13 indicates two dimensional (d = 2) nature of particle trajectory (motion in x- and y- direction).

Diffusion coefficient: Histogram of particle displacements

A sample of displacements is obtained from multiple particle trajectories at different lag times. Ignoring the trajectory generating a particular particle displacement allows us to consider all displacements (for a given lag time) as one sample. Therefore, a histogram of displacements for different lag times can be generated. The calculation of MSD includes a time average, since displacements were created at different time points along a trajectory, and an ensemble average, since the displacements come form different particle trajectories. This is known as the "Van Hove correlation function" and it is specified for a given lag time.

$$P(\delta|\tau) = P_0(\tau)\exp\Big(-\frac{|\delta - \delta_0|^2}{\Delta^2(\tau)}\Big) \tag{2.14}$$

where,
$P(\delta|\tau)$ - Probability that a particle covers a distance δ over lag time τ
$P_0(\tau)$ - Normalization constant
δ_0 - Drift in particle sample, due to bulk flow
$\Delta^2(\tau)$ - Variance of the fitted distribution

The variance of the Gaussian curve fitted over the histogram of displacements gives the diffusion coefficient. As mentioned before, greater the number and length of trajectories, greater will be the number of displacements and therefore the calculation of ensemble MSD will be more precise.

2.1.3. Error Analysis

Bias in particle location

The centroid location algorithm is used to refine the location of intensity peaks in particle image. It has to be ensured that there is no bias in the corrected particle location. For instance, when feature size ($2w$) is made too small, the corrected coordinates might be rounded off to the nearest integer. One way to check for bias is by plotting a histogram of x- and y-positions. If the histogram does not show any peaks at the ends (0 and 1) and no peak at 0.5, but appears flat, it proves that there is no bias in the position correction [7]. Figure 2.2 shows a flat histogram implying no bias in particle location correction.

Static error

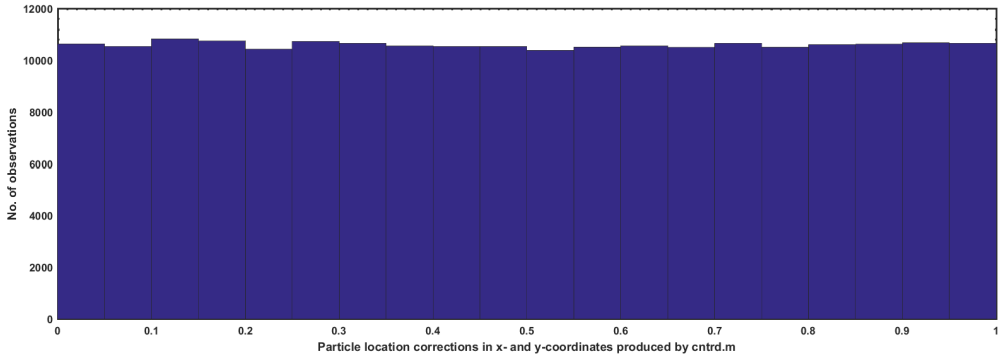

Figure 2.2: Histogram of particle positions (x,y) to identify the bias in centroid location algorithm

Static error can be defined as an intrinsic error in the determination of particle position due to the underlying noise in the experimental setup [8]. This error is estimated by performing position measurements of immobilized particles. The MSD values obtained upon performing the measurement are constant against the lag time. The static error is corrected by discarding all values of MSD that are lesser than or equal to the measured constant error value. This is logical because any value of MSD lesser than the static error make no physical meaning.

Statistical error

A simple estimate of statistical error is provided by the following equation[**?**]

$$\%\,Error = (\frac{1}{\sqrt{N_{disp}}})100 \tag{2.15}$$

where,
N_{disp} - Number of particle displacements

Error in linear curve fitting

The Mean Squared Error (MSE) associated with the estimated value of slope is given by equation [12]

$$MSE = \sum_{i=1}^{n} \frac{(y_i - \hat{y})^2}{n-2} \tag{2.16}$$

where,
y_i - Measured value
$\hat{y}$ - Mean value
n - Number of observations

Drift correction

Based on the thermal state of the room, experimental setup and stage, some creeping flow may enter the sample and affect all the particle trajectories. In this report, we assumed that the drift in the sample was homogeneous and hence, displacement due to the drift would be the same for all particles at any given point. One way to identify the drift is by plotting the x- and y-positions of all the selected particle trajectories. A constant increase/decrease in the particle position over time indicated the presence of drift. In such a situation, the particle displacement was due to Brownian motion and a constant drift. This drift is corrected by taking a mean of the displacements of the identified particle trajectory. Ideally since the particle is undergoing Brownian motion, mean of

displacements should be zero (in the absence of any other systematic error) but in the presence of drift, a constant value would be obtained as a result. This value can be subtracted from the particle positions in a trajectory. One must remember that tampering with the raw data can result in more errors. Furthermore, this technique works when drift is homogeneous however that is an ideal scenario.

2.2. Experiment

2.2.1. Sample preparation

5 μL of dilute aqueous polystyrene suspension of different sizes (ϕ 0.22 μm, ϕ 1.337 μm, ϕ 1.89 μm) is placed on a glass slide (24 × 40 # 1.5). A double sided tape is taken. The tape is cut into a hollow rectangle shape and placed on the glass slide to act as a spacer (thickness 150 μm). A cover slip (24 × 50 mm # 1) is placed on the glass slide to cover the liquid and form a closed chamber. The closed chamber is sealed by applying a thin layer of UV-curing glue on the edges of the chamber. The chamber is placed under the UV light for 5 minutes. The chamber is now ready and placed on the stage of the microscope for experiment. Prior to the assembly, both the coverslip and the glass slide are placed in a 1 M NaOH solution for 15 minutes, rinsed with DI water and ethanol, and dried under pressurized air stream. Figure 2.3 schematically illustrates the particle tracking set-up.

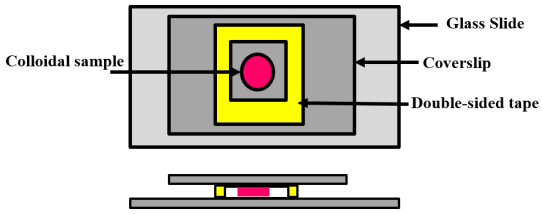

Figure 2.3: Schematic representation of particle tracking set-up

2.2.2. Static error measurement

The experiment to estimate the static error involves tracking immobile particles in a dried up sample using video microscopy. The sample is enclosed between a glass slide and a cover slip as described in the procedure in section 2.2.1. The only difference is that the particles are immobile because all the liquid has dried up. The MSD resulting from the analysis of the immobile particles is called the static error.

2.3. Results and Discussion

2.3.1. Linear fitting: MSD vs Lag time

Figure 2.4 shows the linear increase in MSD with lag time. A linear fit is applied on these curves and the estimated slope is used to determine the diffusion coefficient using equation 2.13. Table 2.1 tabulates the estimated diffusion coefficients. The statistical uncertainty associated with these estimates is less than 1.5%. The estimated diffusion coefficients are plotted against the particle size in figure 2.5. The smooth curve indicates the theoretical diffusion coefficient as a function of the particle size based on the Stokes Einstein equation

$$D = \frac{k_B T}{6\pi\eta r} \tag{2.17}$$

where,
k_B - Boltzmann constant
T - Temperature
η - Viscosity of the medium
r - Radius of the particle

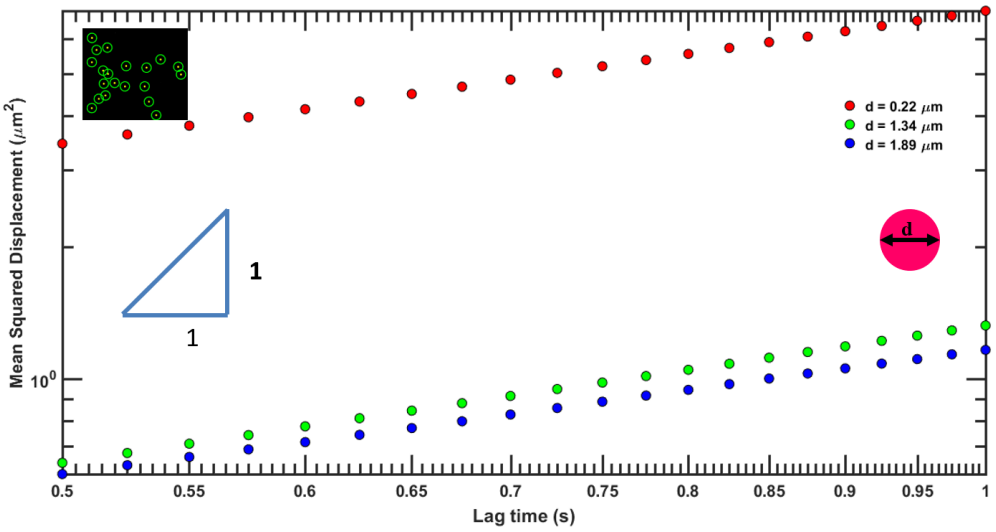

Figure 2.4: MSD vs lag time for particles of different sizes (ϕ 0.22,ϕ 1.337,ϕ 1.89 μm)

Table 2.1: Estimated diffusion coefficient of colloidal particles

Particle size (in μm)	Diffusion coefficient (in $\mu m^2/s$) ± 95% confidence interval
0.22	2.21 ± 0.02
1.337	0.37 ± 0.01
1.89	0.26 ± 0.01

2.3.2. Histogram of particle displacements

A histogram of particle displacments is shown in figure 2.6 to show the effect of lag time on the variance of the distribution fitted on the histogram. The distribution fit becomes wider indicating an increase in the uncertainty of the estimated diffusion coefficient due to poor statistics at longer lag times (less particle displacments).

2.3.3. Correction for Drift

Based on the procedure described in the 2.1.3, the particle trajectories were corrected for drift. Figure 2.7 and figure 2.8 show how a particle trajectory subjected to constant drift changes upon correction.

2.3.4. Correction for static error

The static error is corrected by eliminating all those MSD points that are smaller than or equal to the constant MSD value obtained during the static error experiment. The figure 2.9 shows that the MSD for immobile particles is approximately 0.0006 μm^2. Hence, all MSD values from the particle tracking experiments smaller than or equal to 0.0006 μm^2 were discarded from the analysis.

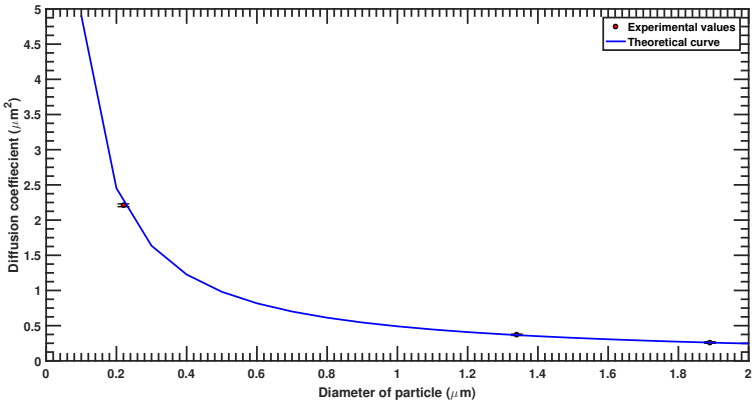

Figure 2.5: Estimated diffusion coefficient against lag time

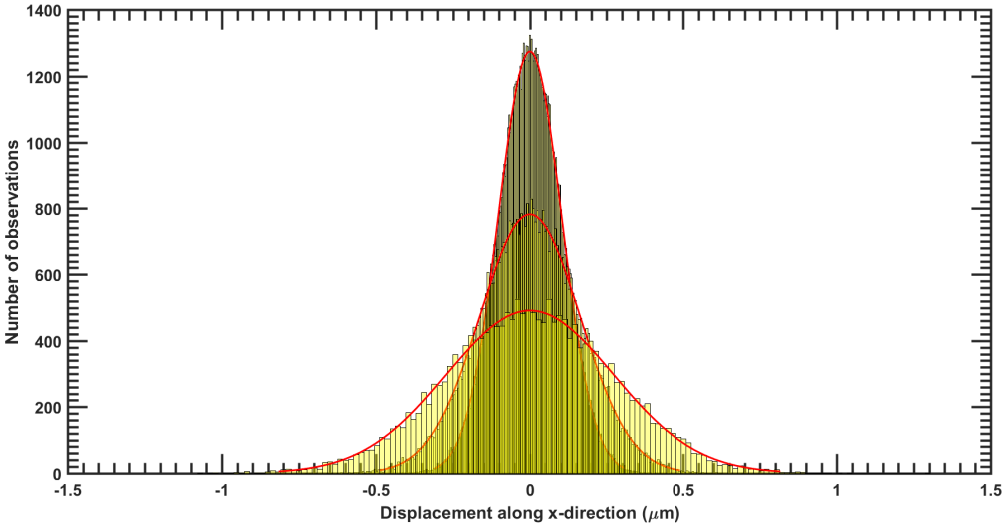

Figure 2.6: Histogram of particle displacements at different lag times

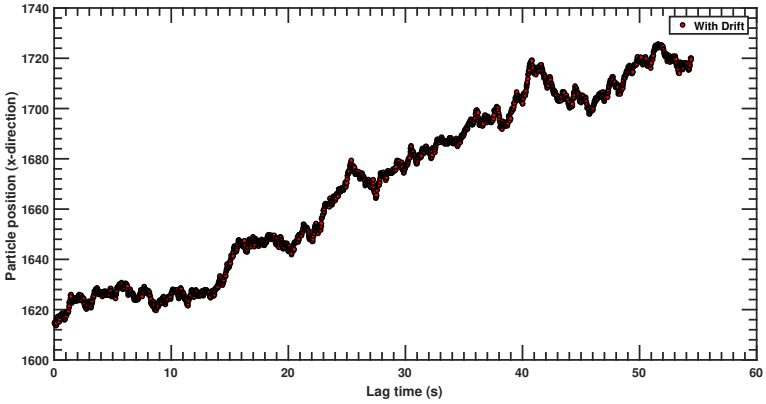

Figure 2.7: Particle positions with drift

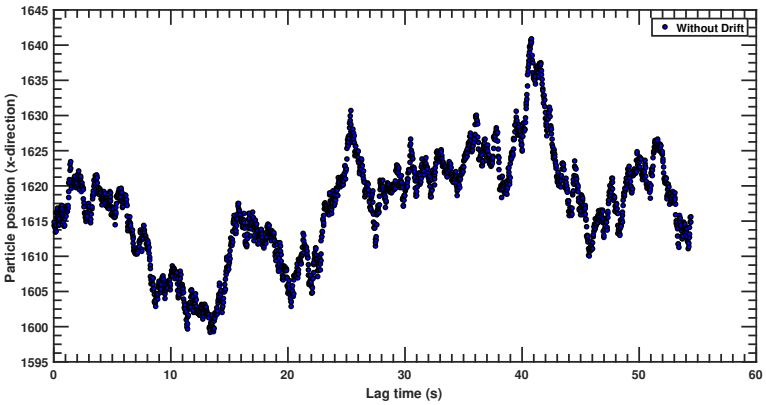

Figure 2.8: Particle positions without drift

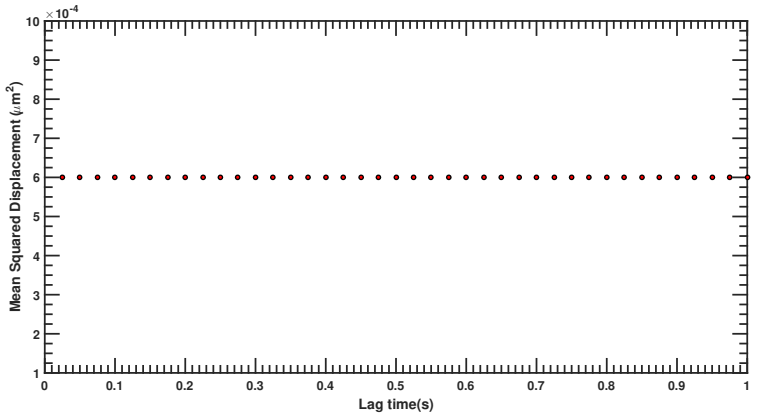

Figure 2.9: MSD vs lag time: Static error determination

3
Colloidal Model

The system can be described as a confined microfluidic channel consisting of multiple PEGDA hydrogel pillars (analogous to deformable wall) with a centre-to-centre separation of approximately 100 μm, fluorescent PS (ϕ1.337μm) colloidal particles (analogous to rigid spheres) and with dextran (M.W. 450,000 to 650,000) as depletant suspended in an aqueous medium. The colloidal particles undergo Brownian motion and it is expected that when the particles are brought closer to the hydrogel post, they experience an attractive interaction force called depletion interaction. When the particles come in contact with the PEGDA post, they deform the post. This energy associated with the deformation is called elastic energy and is a function of the hydrogel elasticity. The combination of elastic energy of deformation and attractive depletion energy results in an energy potential well. The time required by the colloidal particle to escape the potential well is predicted using the Kramer's escape time.

In this chapter, section 3.1.1 discusses the theory of deletion interaction, section 3.1.2 briefly describes the star-polymer fractal network structure of PEGDA hydrogels, section 3.1.3 describes the mathematical expression for elastic energy of deformation, section 3.1.5 explains graphically how a potential well is created due to the combination of depletion interaction and elastic energy of deformation. Finally, section 3.1.6 discusses the concept of escape time and its quantitative expression.

3.1. Theory

3.1.1. Depletion Interaction

Depletion interaction is seen between colloidal spheres in a solution of non-adsorbing macromolecules (called depletants). Negative adsorption on the surface of colloidal particle gives rise to a depletion layer close to the surface of the particle. In this layer, the concentration of the non-adsorbing species (macromolecules) is lower than the average concentration. This does not imply a complete absence of the material within the layer, rather it suggests that the centre of mass of the macromolecule cannot approach the colloidal particle closer than the macromolecules's radius of gyration (R_g) [13]. This volume surrounding the colloidal particles which the macromolecules cannot occupy or are "excluded" from is called excluded volume.

The overlap of excluded volumes of 2 colloidal particles increases the volume accessible to the macromolecules in the bulk. This is because the overlapping part of the depletion layers is now a volume which is free from the depletants. Therefore, their entropy increases (ΔS increases) and since a hard-sphere mixture is an athermal system (process neither involves heat nor change in temperature [14]), their free energy ΔG = -TΔS (2^{nd} law of thermodynamics) decreases [15]. The effect of this is an attractive force between the colloidal spheres even though the direct colloid-colloid or colloid-macromolecule interactions are repulsive [16]. This nature of interaction results in a phase separation of the large colloidal and small macromolecules [17]. Figure 3.1 illustrates the depletion interaction between the hydrogel posts and the colloidal particles suspended in a medium containing depletants.

These mixtures are described in terms of the "volume fraction" (ϕ_{poly}) of the macromolecule coils. The volume fraction is expressed as

$$\phi_{poly} = \frac{n_b}{n_b^*} \tag{3.1}$$

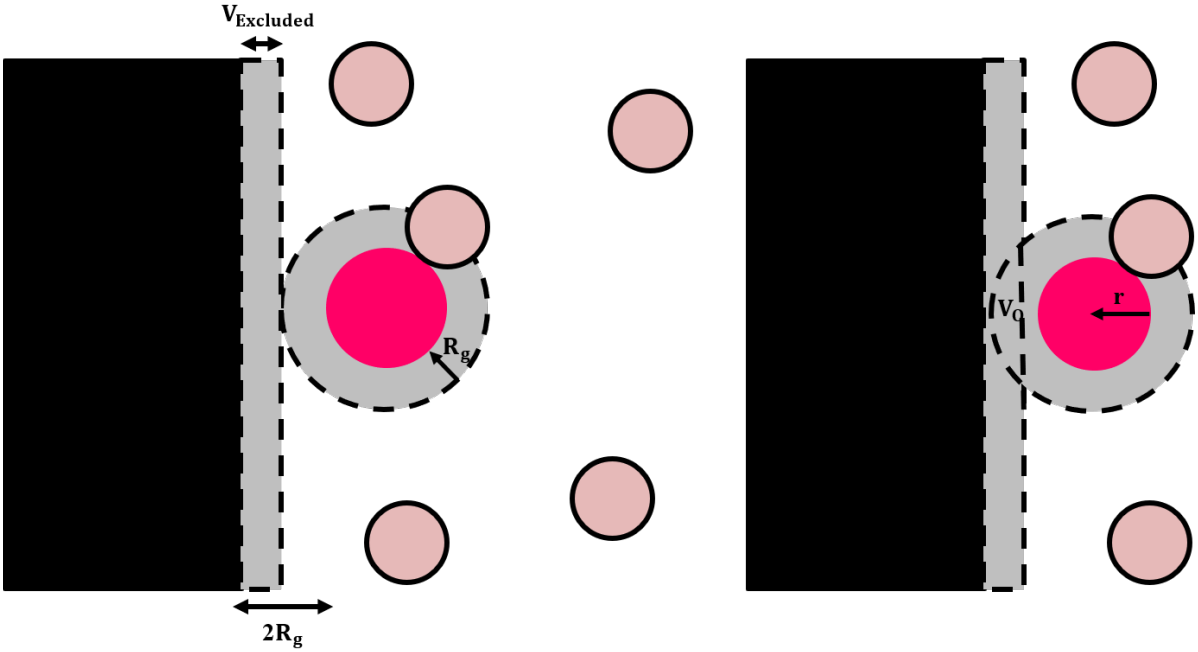

Figure 3.1: Schematic representation of depletion interaction. $V_{Excluded}$ is the excluded volume of the colloidal particle and the post, R_g is the radius of gyration of depletant, V_O is the overlap volume

and

$$n_b^* = \frac{3}{4\pi R_g^3} \tag{3.2}$$

where,
n_b - Number density of the macromolecules in bulk
n_b^* - Number density of macromolecules at which the macromolecule coils overlap

For small depletant concentration (dilute regime, ϕ < 1), the attraction can be expressed as a product of the osmotic pressure and the overlap volume [18][19]. When ϕ exceeds one, the system enters into the semi-dilute concentration regime.

$$F = K_B T N \frac{\partial ln Q}{\partial h} \tag{3.3}$$

$$Q = \int_x \exp \frac{-w(x)}{K_B T} dx \tag{3.4}$$

where,
F - Depletion force
$K_B T$ - Thermal Energy
N - Total number of macromolecules in the system
h - Gap width between the particle and plate (or surface to surface separation)
$w(x)$ - Free energy of a macromolecule located at position x
For the case of purely hard particles and macromolecules (i.e. only hard sphere interactions), Q will be given by the total free volume available to the macromolecules. So, equation 3.4 can be re-written as

$$F = \frac{K_B T N}{V_{free}} \frac{\partial V_{free}}{\partial h} = K_B T (\frac{N}{V_{free}}) \frac{\partial V_{free}}{\partial h} \tag{3.5}$$

where,
V_{free} - Total free volume available to the macromolecules

When the volume fraction of the particles and the macromolecules is relatively small, the term

$\frac{N}{V_{free}}$ will be approximately equal to the bulk number density of the macromolecules, n_b. Since, the total volume of the system is assumed to be fixed, we can write

$$V_{Free} = V_{Total} - V_{Excluded} \tag{3.6}$$

$$F = K_B T n_b \frac{\partial V_{Total} - V_{Excluded}}{\partial h} = -K_B T n_b \frac{\partial V_{Excluded}}{\partial h} \tag{3.7}$$

$$F = -K_B T n_b \frac{\partial V_{Excluded}}{\partial h} \tag{3.8}$$

$V_{Excluded}$ - Volume of system excluded from the macromolecules (= overlap volume)

The negative sign in 3.8 implies an attractive force.
The expression for overlap volume between the colloidal particle and the wall is given by

$$V_{Excluded} = V_O = \pi(2R_g - h)^2 \left[r + \frac{h}{3} + \frac{R_g}{3} \right] \tag{3.9}$$

where,
h - Surface to surface separation between colloidal particle and the wall
r - Radius of colloidal particle
V_O - Overlap volume

A detailed derivation of the overlap volume is given in appendix A.

A hypothetical model depletant behaves as a penetrable hard sphere. It mimics an ideal macromolecule. The model is characterized by the fact that the spheres freely overlap each other but act as hard spheres with diameter σ when interacting with the wall or the colloidal particle. Since penetrable hard spheres behave thermodynamically ideally, the osmotic pressure acting from the outside is given by the Van't Hoff's law

$$P_{osmotic} = K_B T n_b \tag{3.10}$$

The depletion energy can be obtained by integrating C.6 over h. So,

$$W = P_{osmotic} V_{overlap} = K_B T n_b \left(\pi(2R_g - h)^2 \left[r + \frac{h}{3} + \frac{R_g}{3} \right] \right) \tag{3.11}$$

3.1.2. Structure of PEGDA hydrogels

PEGDA hydrogels in water are used in this project to form cylindrical posts in the microchannel and serve as deformable walls. These hydrogels have a highly heterogeneous structure comprised of star-like polymers arranged in a fractal network. This structure is formed by the binding of polyethyleneglycol chains (PEG) to the bi-functionalized diacrylic backbone [20].

Polymer stars inter-connect with each other to form a fractal network which results in the formation of 2 phases: polymer-rich phase and polymer-lean phase (called voids). The size of the voids is of the order of 10 to 100 nm. The smallest length scales correspond to small subsections of the individual polymer chains with size ξ. The largest length scales correspond to the size of voids in the fractal network, Ξ.

The fraction of the network phase increases with the increase in polymer concentration consequently resulting in formation of a homogeneous hydrogel. The molecular weight of the polymer does not have a significant impact on the homogeneity of the hydrogel. Hence, it is not surprising to observe an increase in the linear elastic modulus (G_0) of the hydrogel with increase in total polymer concentration (ϕ_0). The elastic shear modulus decreases with increasing heterogeneity [20].

PEGDA hydrogels are used commonly used for lab scale research applications [21], biological applications to mimic tissues [22] due to their economic costs and easy availability. These hydrogels are prepared by photo-crosslinking using photoinitiator (PI) with UV light. This permits control over the size, shape and elasticity of the hydrogel [23]. Figure 3.2 illustrates the microscopic structure of the PEGDA hydrogel.

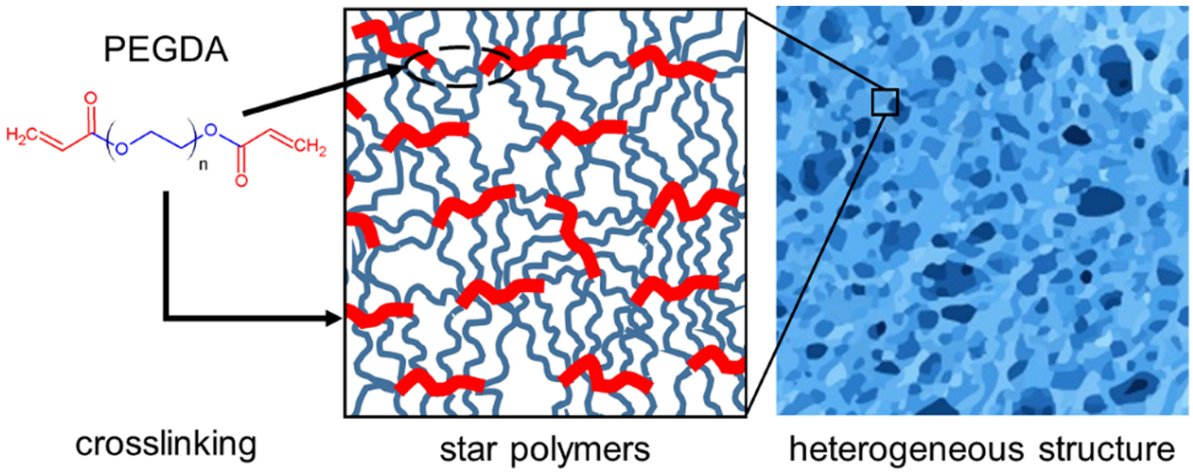

Figure 3.2: Schematic representation of depletion interaction. Red chains represent the diacrylic backbone, Blue chains represent PEG polymer [20]

3.1.3. Energy of deformation

The deformability of the PEGDA posts is a function of their elasticity or elastic modulus. Photo-crosslinked polymer hydrogels exhibit a neo-hookean behaviour [24] which means that the stress and strain relationship is initially linear but it reaches a plateau at some point [25]. However, for a simplistic model, we assume that the hydrogel posts behave as isotropic hookean solids. This implies that the stress-strain relationship is linear and the elasticity of the hydrogel is same in all directions. The contact between a rigid sphere with radius R (colloidal particle) and a deformable wall (PEGDA post) results in a force required to deform the wall [26]. The order of magnitude of elastic deformation is

$$\epsilon \approx \frac{d}{2a} \tag{3.12}$$

where,
ϵ - Elastic deformation
d - Length of deformation of the wall (= penetration depth)
$2a$ - Contact diameter between the sphere and the wall

Hence, the magnitude of stress (σ) based on Hooke's law is [27]

$$\sigma = \epsilon E = \frac{d}{2a} E \tag{3.13}$$

where,
E - Elasticity of the deformable wall

Since stress is defined as force per unit contact area (A), the magnitude of deforming force, F, is

$$F = \sigma A = \frac{E(\pi a^2) d}{2a} = \frac{Ed\pi\sqrt{2Rd}}{2} \tag{3.14}$$

$$F = \frac{4}{3} E d^{\frac{3}{2}} R^{\frac{1}{2}} \tag{3.15}$$

Using equation 3.15, we can obtain the expression of elastic energy by integrating the force over the deformation length (d). Therefore,

$$U = \frac{8}{15} E d^{\frac{5}{2}} R^{\frac{1}{2}} \tag{3.16}$$

A more detailed explanation of the deforming force and elastic energy is provided by [26].

3.1.4. Elasticity of hydrogel

The elastic energy of deformation can be calculated by estimating the elasticity of the PEGDA posts [27]. The elastic modulus of a viscoelastic material can be expressed as

$$E = E^{'} + iE^{"} \tag{3.17}$$

where,
$E^{'}$ - Tensile storage modulus (= $E\cos\delta$)
$E^{"}$ - Tensile loss modulus (= $E\sin\delta$)
δ - Phase lag or phase angle between stress and strain

The shear modulus can be expressed as

$$G = G^{'} + iG^{"} \tag{3.18}$$

where,
$G^{'}$ - Shear storage modulus (= $G\cos\delta$)
$G^{"}$ - Shear loss modulus (= $G\sin\delta$)

The storage modulus is a measure of the storage energy (i.e. elastic part) and loss modulus is a measure of the energy lost as heat (i.e. viscous part).

For an isotropic, hookean solid, elasticity can be expressed as

$$E = G = G^{'} + iG^{"} \tag{3.19}$$

This implies that measuring the shear elastic modulus (G) allows us to also measure the elasticity (E). The concept of elasticity as function of storage and loss modulus is explained in detail in [27]

3.1.5. Energy Potential: Depletion energy and Energy of deformation

The system deals with the 2 competing energies: Depletion energy (attractive force pushes the particle towards the post) and elastic energy of deformation (pushes the particle away from the post upon contact). These two energies together result in a potential energy well. Figure 3.3 describes the energy potential well. In this figure,

1. Path (e) - (c) - Particle is approaching the hydrogel post
2. Path (c) - (d) - Particle is in contact with the hydrogel (Surface to Surface separation is zero)
3. Path (b) - (a) - Particle is pushing into the hydrogel post and is deforming the post

In this well, the potential energy of the particle decreases as it moves closer to the wall due to the attractive force, reaches a minimum indicating a binding event and then increases as the elastic energy pushes the particle away from the post.

The shape of this potential well, of which the depth is of particular interest, depends on factors influencing the depletion energy and elastic energy [4]. Therefore,

1. Radius of gyration of depletant - For a given volume fraction of depletant, as the size of depletant decreases the number of depletant particles increases. Since, depletion force is an entropic force, an increase in the depletion energy is observed.
2. Size of colloidal particle - The depth of energy potential increases with increase in the size of colloidal particle due to stronger depletion force.
3. Volume fraction of depletant - As the volume fraction of depletant increases, the depth of energy minimum increases due to stronger depletion forces.
4. Elasticity of the hydrogel post - As the elasticity of the hydrogel post increases, the depth of energy potential decreases since energy for deformation increases.

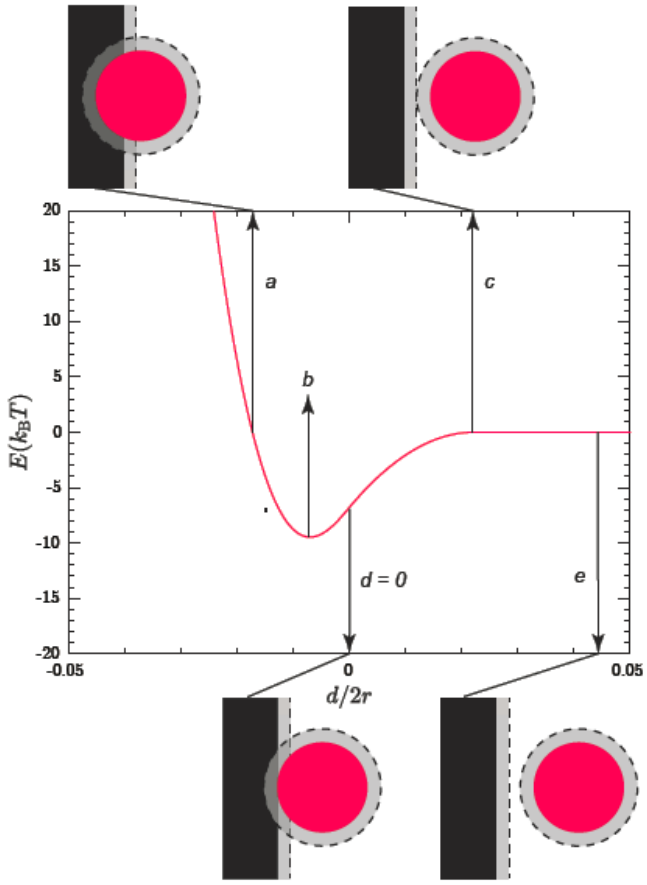

Figure 3.3: Graphical representation of the energy well [4]

3.1.6. Escape Time

Escape time is an indirect measure of the depth of the energy potential. The time required by the particle to come out of the potential well is called escape time.

The escape time will depend on factors influencing the depth of the energy potential well. It will decrease with increasing elasticity of post, decreasing size of colloidal particle and it will increase with increase in concentration of depletant within the dilute regime [4].

3.2. Experiment

Table 3.1 tabulates all the chemicals used in the project for preparing microfluidic devices, hydrogel posts and the colloidal particle suspension. All chemicals were directly used as supplied by the manufacturer. The water used in all the experiments is de-ionized water supplied by the department of process and energy.

3.2.1. Microfluidic device preparation

Preparation of the silicon wafer

A silicon wafer is used as a mould for preparation of the chips. The wafer should be hydrophobized if it is new or has been used at least 10 - 15 times. The mould is washed with 0.1 M NaOH solution for 15 minutes and then dried under nitrogen flow to remove any dust. 10 drops of silanzing agent are placed in a small vial. Both the wafer and the vial are then placed inside a dessicator for 2 hours. The pressure inside the dessicator is reduced to less than 100 mbar. After 2 hours, the pressure inside the dessicator is brought back to atmospheric pressure and the wafer is carefully

Table 3.1: List of chemicals

Abbreviation	Full Form	% Purity	Supplier
PEG M.W. 2000	Polyethyleneglycol M.W. 2000	-	Sigma Aldrich
PEGDA M.W. 700	Polyethyleneglycol diacrylate M.W. 700	-	Sigma Aldrich
PEGDA 6000	Polyethyleneglycol diacrylate M.W. 6000	<1500 ppm MEHQ	Sigma Aldrich
TPM	3-(Trimethoxysilyl)propyl methacrylate	98%	Sigma Aldrich
NaCl	Sodium Chloride	-	-
NaOH	Sodium Hydroxide	≥ 97%	Sigma Aldrich
Darocur	2-Hydroxy-2-methylpropiophenone	-	Sigma Aldrich
-	Sylgard 184, silicone elastomer	-	Dow
-	Sylgard 184, curing agent	-	Dow
EtOH	Ethanol	-	-
PS	Polystyrene microspheres	2.5% solids in water	Polysciences Inc.
-	Dextran M.W. 450,000-650,000	-	Sigma Aldrich

removed.

Preparation of the PDMS mixture

A pdms mixture is generated by using Sylgard 184 kit containing PDMS monomers and a curing agent. 5 g of the curing agent is mixed with 35 g of the PDMS monomer in a falcon tube to produce roughly 5 mm layer of PDMS mixture on the wafer. These components are mixed vigorously using a spatula until the resulting mixture is completely opaque due to bubble formation. The mixture is centrifuged at 7400 rpm for 15 minutes to settle down any dust and the bubbles.

Preparation of the mould

The PDMS mixture is poured slowly and evenly over the wafer. The mould is left inside the vacuum chamber for 30 minutes to get rid of the bubbles. The pressure inside the chamber is reduced to 40 mm of Hg. The mould is placed inside the oven at 65 °C overnight. The mould is cut from the silicon wafer carefully using a sharp razor blade. Then, the mould is placed on a clean petri dish feature side up.

Preparation of the microfluidic chip

The mould is put feature side up on a white background. A scalpel is used to make incisions into the mould and 3-5 mm away from the device features. It is ensured that the scalpel is always placed vertically into the mould to make clean cuts. The chip is scooped up using the scalpel and lifted out of the mould, held only by the edges. The chip is placed feature side up on a clean petri dish.

Inlet and Outlet ports in the device

Luer stubs are used to create inlet and outlet ports in the microchip. The luer stubs are carefully placed on the inlet and outlet feature of the chip. A constant pressure is applied on the stubs to push them all the way down into the PDMS. The PDMS bore is pulled out from the stub. The stub is screwed out of the chip by a twisting motion. The chip is cleaned and placed back on the petri dish feature side up.

Preparation of the glass slides

A glass slide (24 × 50 mm #1.5) is used to provide a base to the devices. These slides are cleaned by placing them inside a falcon tube filled with 1 M NaOH solution. 1 M NaOH solution is prepared

by dissolving 4 g of NaOH in 100 ml of water. The slides are left inside the solution for 30 minutes after which the NaOH solution is replaced by water. The slides are left in water for 5 minutes. Finally, the slides are dried under pressurized air. The slides which are not used immediately are stored in water.

Preparation of the microfluidic device

The microchip is cleaned before placing it on the glass slide. The chip is placed inside a falcon tube and the tube is filled with ethanol. The tube is placed inside an ultrasonic bath for 20 minutes. The ethanol is replaced by water in the falcon tube and the tube is placed in the ultrasonic bath for another 20 minutes. The chip is taken out of the tube with the help of tweezers and dried using pressurized air. The chip is picked from its edges using the tweezers and placed carefully on the glass slide. Care is taken to avoid pressing the chip on the slide to prevent delamination. The assembled device is put into the oven at 65 °C for 2 hours to remove any delamination.

Functionalization of the microfluidic device

The microfluidic device is functionalized using TPM to enhance the binding of the PEGDA posts on the glass slide. The functionalizing liquid, having concentration 25 mg/mL, is prepared by dissolving 75 mg of TPM (72 μL) in 3 mL of ethanol. The device is taken out of the oven and allowed to completely cool down. It is cleaned by first passing water at 0.07 bar and then by passing air at 0.07 bar using a pressure gauge. After the channel is cleaned, it is filled with 1 M NaOH solution at 0.07 bar using the pressure gauge and the device is left for 1 hour. It is cleaned by passing water at 0.07 bar and then by passing air at 0.07 bar. Once the device is cleaned, the channel is filled with acrylate solution at 0.07 bar and is left for 30 minutes. The device is cleaned by first passing ethanol at 0.07 bar and then by passing air at 0.07 bar. Finally the device is put into the oven at 65 °C overnight.

Figure 3.4 shows the image of the microfluidic channel as viewed under the microscope and figure 3.5 illustrates the steps involved in microfluidic device preparation.

Precautions

Certain precautions must always be taken when working with microfluidic devices to prevent dust accumulation inside the channel, leakages, and any accidental damage: -

1. All work must be carried out inside the fumehood to prevent dust from entering inside the channel.

2. Gloves must always be worn when handling microfluidic devices.

3. Ensure that all fluids passed into the channel are freshly prepared.

4. The chips should not be pressed on the microscopic slides during assembly.

5. The device should be put into the oven for 2 hours to remove delamination.

6. If the device was put into the oven, no fluid should be passed into the channel until the device has completely cooled down.

7. The microfluidic device should be cleaned to remove any pollution. The device was cleaned by placing it inside a falcon tube and filling the tube with ethanol. The tube is sonicated in the ultrasonic bath for 20 minutes. The ethanol is then replaced by water and the tube is sonicated for another 20 minutes. After this the device is removed from the falcon tube and dried under pressurized air stream.

Figure 3.4: Microfluidic channel

3.2.2. Hydrogel post preparation

Preparation of the hard post mixture

An eppendorf tube is cleaned and wrapped with aluminium foil to prevent cross-linking of the mixture due to light. PEGDA 700 solution is taken out of the fridge and brought to the room temperature. 990 μL of PEGDA 700 and 10 μL of darocur were added into the eppendorf tube. This mixture was homogenized by mixing it using a vortex mixer for 15 minutes followed by sonication in the ultrasonic bath for 15 minutes. The mixture can be stored inside the refrigerator at 4 °C.

Preparation of the soft post mixture

An eppendorf tube is cleaned and wrapped with aluminium foil to prevent cross-linking of the mixture due to light. A pre-hyrogel mixture is prepared by adding 12 wt% PEGDA 6000, 20 wt% PEG 2000 and 68 wt% water inside the eppendorf tube. This mixture is homogenized by mixing it using the vortex mixer for 15 minutes followed by sonication in the ultrasonic bath for 15 minutes. It is essential to ensure that the mixture is completely homogenized. Once the pre-polymer mixture is prepared, 10 μL of darocur is added into the eppendorf tube. This mixture is homogenized by mixing it using the vortex mixer for 15 minutes followed by sonication in the ultrasonic bath for 15 minutes. The mixture can be stored inside the refrigerator at 4 °C.

Synthesis of posts

The post mixtures are taken out of the refrigerator and brought to the room temperature. The mixtures are homogenized by placing them in an ultrasonic bath for 15 minutes. The microfluidic device is taken out from the storage and cleaned to remove any pollution. If the channel is delaminated, the device is placed inside the oven for 2 hours.

The hard post mixture is passed through the channel at 0.07 bar using the pressure gauge. The device is placed on the stage of the Nikon T*i*-E microscope and viewed, under the BF mode, to decide the location of the PEGDA posts. At first, small posts (ϕ40 μm) are made by illuminating UV light, 600 times for a period of 0.1 s with a wait time of 0.05 seconds at a distance of 5 μm away from the bottom of the channel, through a circular ϕ1000 μm photomask at 40x magnification. Once the small hard posts were prepared, ϕ1000 μm photomask is replaced by ϕ2300 μm photomask to produce desired number of large (ϕ100 μm) hard posts around the small posts using the same

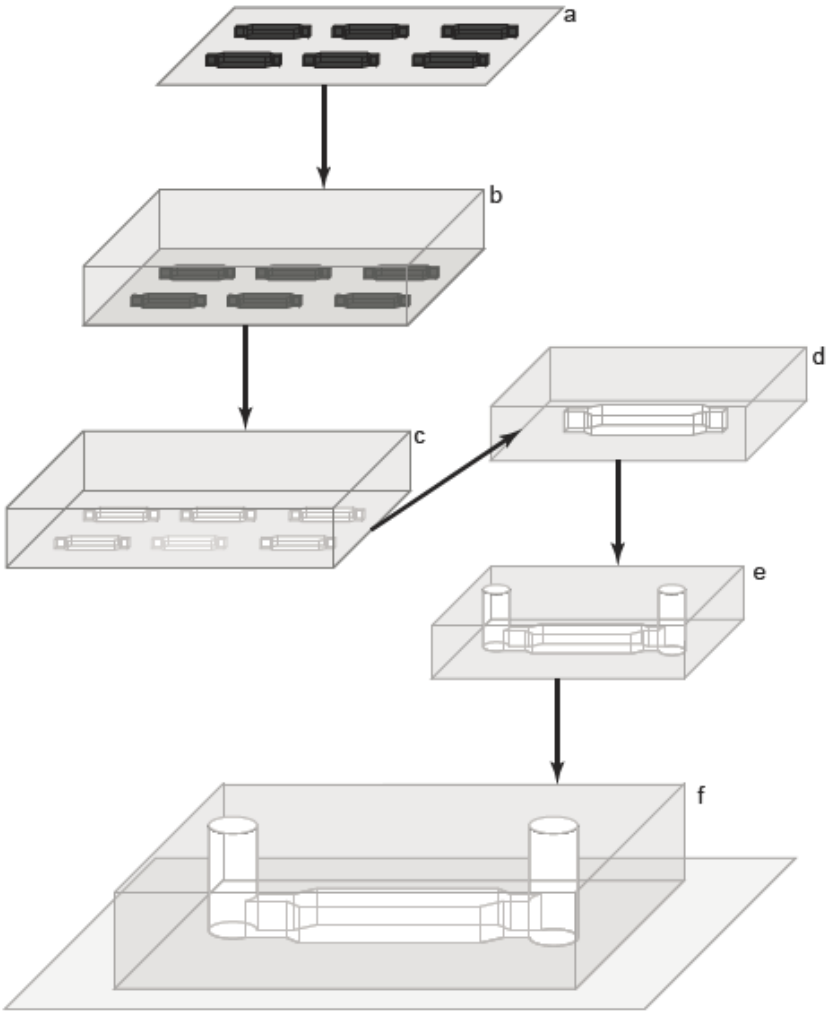

Figure 3.5: Steps involved in microfluidic device preparation [4]. (a) Preparing the silicon wafer, (b) Pouring the PDMS mould over the wafer, (c) Removing the PDMS mould from the wafer, (d) Cutting the PDMS mould to obtain single channel, (e) Creating inlet and outlet ports in channel, (f) Placing the channel on the glass slide

exposure time as that for the small hard posts. The channel is rinsed by passing water at 0.07 bar using the pressure gauge. The channel is filled with the soft post mixture at 0.07 bar using the pressure gauge. The desired number of soft posts are created around the small hard posts by illuminating the UV light, 30 times for a period of 2 s with a wait time of 0.1 seconds at a distance of 5 μm away from the bottom of the channel, through the ϕ2300 μm photomask. Once the desired number of soft posts are synthesized, the channel is rinsed with water. The microfluidic device is placed under a UV lamp for 1.5 hours to cure the hydrogels and achieve maximum cross-linking. The device is then preferably immediately used for experiments. If required, the device can be stored in a falcon tube filled with water. The UV light is generated using Nikon Intensilight C-HGFI at 50% of the total light intensity. Figure 3.6 and 3.7 represent the hard and soft hydrogel posts made in the channel.

Precautions

Synthesis of posts can become difficult if following precautions are not taken into consideration: -

1. Posts must not be synthesized if the the post mixture is flowing through the channel. This was not a major problem in case of the hard post mixture since the viscosity of the mixture was high and so, once the channel was filled, the flow was negligible. However, the soft post

mixture was an aqueous solution with low viscosity and so, once the channel was filled synthesis should be started only when there was negligible liquid flow (This generally required a period of 10 minutes). If the soft posts were made while the liquid was still flowing, no visible cross-linking would be observed.

2. Focusing plays an important part in the preparation of the posts. Incorrect focusing might result in unclear and/or larger posts. Furthermore, it might affect the shape of the posts. This means that posts might not be cylindrical but rather conical in shape.

3. The post mixtures passed through the channel should preferably be freshly made. Soft post mixtures that are more than a day old do not show any visible cross-linking for the described exposure time.

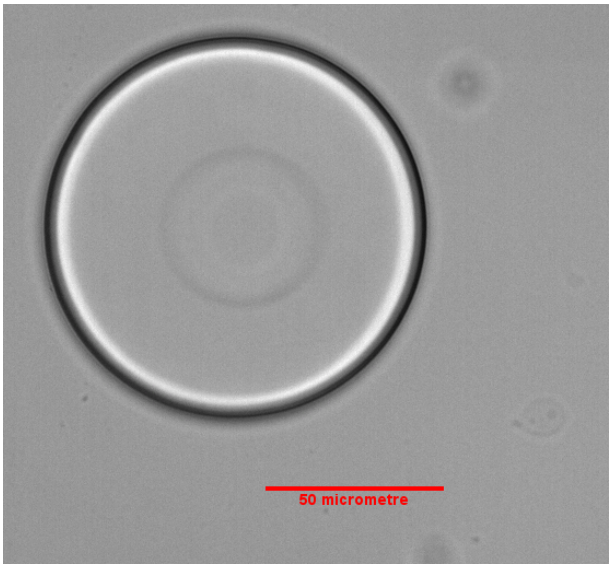

Figure 3.6: Hard Post

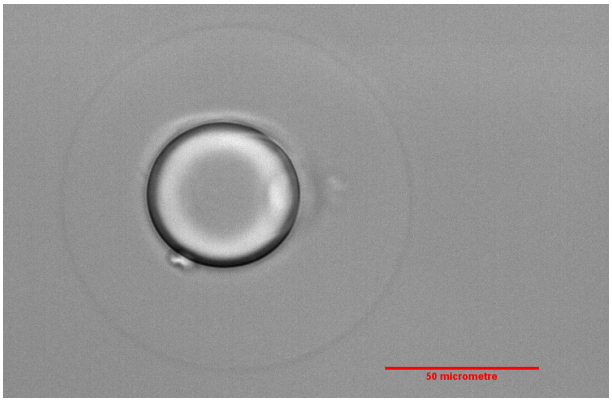

Figure 3.7: Soft Post

3.2.3. Depletion Experiment

Preparation of the particle mixture

The particle mixture for performing depletion experiment is generated by mixing dextran, sodium chloride and diluted polystyrene particle solution. A stock solution for dextran (27.25 g/L) is generated by mixing 545 mg of dextran in 20 mL of water. The stock solution of dextran is passed

through a 200 nm filter. 50 μL of the stock solution is diluted 5 times by mixing it with 200 μL of water to achieve the desired concentration. A stock solution of sodium chloride (50 mmol/L) is prepared by mixing 90 mg of NaCl in 30 mL of water. 50 μL of this stock solution is diluted 10 times by mixing it with 450 μL of water. The stock solution of polystyrene beads is serially diluted to achieve a volume fraction of the order of 10^{-5}. The experimental mixture is prepared by adding 20 μL of 5 mmol/L sodium chloride solution to screen electrostatic interaction (Debye screening length given by equation 3.20), 20 μL of diluted dextran solution (dilute regime $\phi_{poly} < 1$) and 60 μL of diluted polystyrene solution. This mixture is homogenized by placing it inside an ultrasonic bath for 5 minutes.

Performing the depletion experiment

The microfluidic device is taken out of the storage, cleaned and dried under the pressurized air stream. The experimental mixture is passed into the channel at 0.03 bar using the pressure gauge. Once the channel is filled, scotch tape was applied to seal the inlet and the outlet ports of the device. The device is placed on the stage of the microscope. Once the bulk flow of the liquid inside the channel has reduced, an image of the posts was taken, in the BF mode, at the chosen location as the initial reference point. The viewing mode is switched from BF to FITC mode and a video was taken at 1 fps for a period of 1 hour using the ND acquisition. Once the video is captured, another image of the posts is taken, in the BF mode, as the final reference point.

3.3. Results and Discussion

3.3.1. Preparation of hydrogel posts

PEGDA 700 and PEGDA 6000 were used to make the hard and the soft posts respectively. The hard post mixture resulted in formation of hard posts consistently In the previous work [4], it was suggested that the soft hydrogel posts can be consistently made by maintaining a PEGDA 6000 concentration of 4 wt% in the soft post mixture. However, this turned out to be incorrect. So, experiments were performed using concentration of 6 wt%, 8 wt% and 12 wt%. Finally, it was observed that the soft posts can be created consistently by maintaining a PEGDA 6000 concentration of 12 wt%. It was also observed that the intensity of the UV light must be maintained at ND2 level (50 % of total light intensity) with an ND2 filter placed in the path of light.

3.3.2. Depletion Experiment using video microscopy

Only one run of the depletion experiment using video microscopy was performed. The technique was discarded due to the poor statistics observed in the previous work [4].

$$\lambda_D = \sqrt{\frac{\epsilon K_B T}{2(Ze)^2 C_{equi}}} \tag{3.20}$$

where,
λ_D - Screening length
Z - Ionic charge
e - Charge of electron
C_{equi} - Concentration of salt in bulk
Figure 3.8 and 3.9 show the depletion experiment in BF and EPI mode.

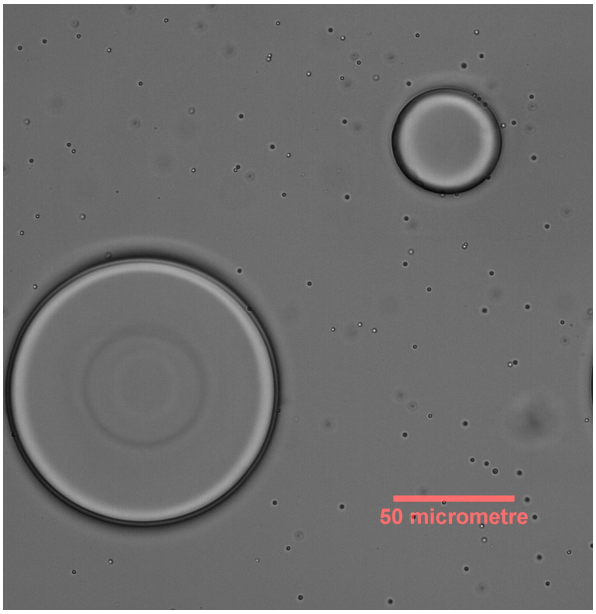

Figure 3.8: Depletion interaction using video microscopy BF mode

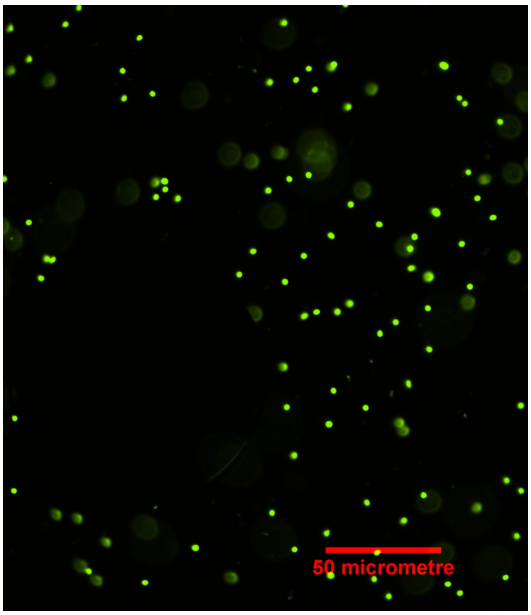

Figure 3.9: Depletion interaction using video microscopy FITC mode

4
Optical Tweezers

Optical tweezers are devices that are used to apply piconewton-sized forces and make measurements of the order of nanometers by applying a focused laser beam on dielectric particles [28]. Optical tweezers have been used for various applications such as particle or cell sorting [29][30], detection and characterization of inter-molecular bonds [31], to establish force-displacement relations [32], measurement of elasticity of membrane [33], binding and disruption of histones to DNA on a molecular level [34], measurement of short range colloidal interactions [35][36][37] and estimation of membrane stiffness [38].

In this project, Zeiss Axio Observer D1 semi-motorized microscope with a diode pumped solid-state Infrared (IR) Nd:YAG laser is used for trapping a colloidal particle in the z-direction (normal to the bottom of the microfluidic chip) and move the particle near the PEGDA post to precisely measure the depletion forces between the particle and the post. The tweezers provide a more controlled environment, by constraining the motion of the particles in the normal direction, than simple tracking of the particles using video microscopy. They offer the possibility to develop a reliable plot of interaction potential against distance from the post and consequently measure the escape time.

In this chapter, the theory behind optical trapping is discusssed in section 4.1. A brief explanation is provided on the calibration of the optical tweezer set-up, automated measurement of the forces, analysis of the measurement errors in section 4.2. The precautions to be taken while performing the experiment and problems faced during the experiment are discussed. The chapter is concluded with the results of the control and depletion experiment based on the force vs displacement curves in section 4.3.

4.1. Theory

4.1.1. Optical trapping

Let us consider a sphere (whose refractive index is larger than that of the surrounding medium) placed in a gradient of light intensity. The light passing through the sphere will be refracted twice due to the change in refractive indices at the 2 interfaces. This change in the path of light results in a change in the momentum of light and consequently, based on Newton's 2^{nd} law, change in the momentum of the sphere. The force exerted by the light on the sphere is proportional to the number of photons in the light and therefore to the local light intensity. The force, due to all the rays of the light, is directed towards to the point of highest intensity. This force is referred to as the "gradient force" due to the gradient in the electric field that produces the force. Another force that acts on the sphere by the virtue of reflection and scattering of light incidented on the sphere is called the "scattering force". This forces causes a radiation pressure on the sphere in the direction of propagation of the beam. Unlike the gradient force, this force is dependent on the light intensity. Optical trapping is achieved when the gradient force is greater than the scattering force. This is achieved by the use of objectives with high numerical aperture (abbreviated as NA) [39]. The trapping force (F) can be given by the following equation

$$U = -P \bullet E = -\alpha E \bullet E \propto -I \tag{4.1}$$

Therefore,

$$F \propto \nabla I \tag{4.2}$$

where,
U - Energy produced by the electric field
P - Dipole moment in the sphere induced by the light
E - Electric field
I - Intensity of the light
α - Polarizability of the light

This force depends on beam waist, intensity of the light, NA of the objective, refractive index and size of the particle. The basic theory behind optical trapping is explained in the figure 4.1

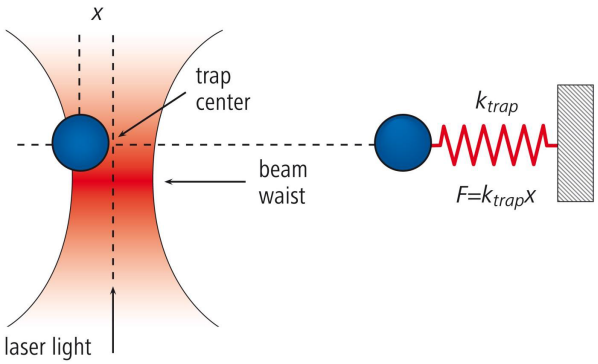

Figure 4.1: Basic working of optical tweezer [40]

4.1.2. Calibration

The calculation of forces exerted by the trap requires estimation of a key parameter: trap stiffness (denoted by k). An optical trap can be visualized as a spring-mass system. When the mass is pulled away from/ pushed into the spring, it experiences a restoring force towards its equilibrium position. This restoring force is linearly proportional to the stiffness of the spring. For small displacements (denoted by Δx) from the equilibrium position, the optical trap is considered to be a harmonic potential [39]. This implies that the trapped particles experience a restoring force (F_{rest}) given by

$$F_{rest} = -k\Delta x \tag{4.3}$$

The system must be calibrated to determine the stiffness of the optical trap. One of the methods for calibrating the system, used in this project, is the "Stokes-Drag" calibration method. According to this method, the force experienced by the particle during calibration is equal to the drag force experienced by the sphere as it moves in a fluid [39]. So, equation 4.3 can be modified to

$$F_{rest} = -k\Delta x = 6\pi\eta r v \tag{4.4}$$

where,
η - Viscosity of the medium
r - Particle radius
v - Constant particle velocity

However, when the particle is in close proximity with the surface, equation 4.4 does not apply and Faxen's law has to be used to determine a correction factor (g) for the Stokes law [41].

$$g = 1 - (\frac{9}{16})(\frac{r}{h}) + (\frac{1}{8})(\frac{r}{h})^3 - (\frac{45}{256})(\frac{r}{h})^4 - (\frac{1}{16})(\frac{r}{h})^5 \tag{4.5}$$

where,
h - Distance of the centre of the sphere from the wall

Error Analysis

The calibration of the system results in a trap stiffness in the x- and y-directions using equation 4.4. The uncertainty associated with the estimated trap stiffness is calculated using

$$k = \frac{6\pi\eta r v}{\Delta x} \tag{4.6}$$

Therefore,

$$\frac{\Delta k}{k} = \sqrt{(\frac{\Delta x}{x})^2 + (\frac{\Delta \eta}{\eta})^2 + (\frac{\Delta r}{r})^2 + (\frac{\Delta v}{v})^2} \tag{4.7}$$

4.1.3. Force measurement

The experiment can be performed once the trap stiffness is determined. Before every experiment, it is necessary to get a reference position for the trapped particle. The system gets the reference position automatically by moving the trapped particle back and forth at different stage velocities. After obtaining the reference position, the particle is moved towards the post, and the position of the trapped particle is calculated automatically by the computer based on the image analysis. Based on the reference position and the position of the particle as it is moved in the channel, displacement at different points of time is calculated. This displacement along with the estimated trap stiffness (from calibration 4.1.2) is used to calculate the force experienced by the particle using equation 4.3. The reference position and the displacement of the particle from its reference position is illustrated in figure 4.2

Error Analysis

The error in the measured force is calculated using

$$\frac{\Delta F}{F} = \sqrt{(\frac{\Delta x}{x})^2 + (\frac{\Delta k}{k})^2} \tag{4.8}$$

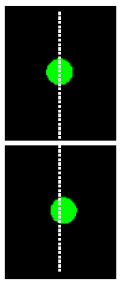

Figure 4.2: Reference position (Top image) and Particle displacement (Bottom image) in optical tweezer [40]

4.1.4. Effect of wall

When a colloidal sphere moving in a quiescent fluid flows near a wall, the Stokes drag force acting on the particle is greater than the drag experienced by the sphere when it is moving far away from the wall. This enhanced drag near the wall reduces the diffusion coefficient of the particle compared to its diffusivity far away from the wall [42].

The drag on the motion of sphere enhances by virtue of the hydrodynamic interactions between the sphere and the wall. These interactions are generated due to the boundary condition imposed by the wall [43]. This effect is illustrated in figure 4.3.

The linearity of the Stokes law permits the drag force experienced by the particle in parallel and perpendicular direction to be separated into 2 independent components.

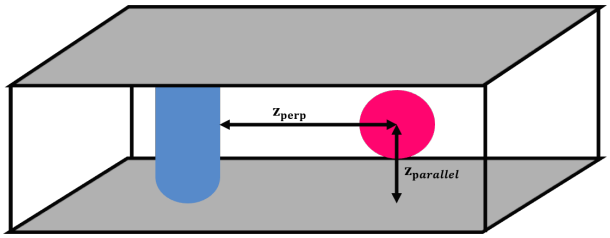

Figure 4.3: Effect of wall

$$F_{||} = 6\pi\eta r v\lambda_{||} = F_{Bulk}\lambda_{||} \tag{4.9}$$

$$F_{\perp} = 6\pi\eta r v\lambda_{\perp} = F_{Bulk}\lambda_{\perp} \tag{4.10}$$

where,
F_{Bulk} - Drag force experienced by the particle as it moves far away from the wall
$F_{||}$ - Drag force experienced by the particle as it moves parallel to the wall
$F_{\perp}$ - Drag force experienced by the particle as it moves perpendicular to the wall
$\lambda_{||}$ - Correction factor to the Stokes drag force as particle moves parallel to the wall
$\lambda_{\perp}$ - Correction factor to the Stokes drag force as particle moves perpendicular to the wall
v - Constant velocity of the particle
η - Viscosity of the medium
r - Radius of the particle

Now, using the Stokes-Einstein equation, the diffusion coefficients can be written as

$$D_{||} = \frac{k_B T}{6\pi\eta r\lambda_{||}} = \lambda_{||}^{-1} D_{Bulk} \tag{4.11}$$

$$D_{\perp} = \frac{k_B T}{6\pi\eta r\lambda_{\perp}} = \lambda_{\perp}^{-1} D_{Bulk} \tag{4.12}$$

where,
$D_{||}$ - Reduced diffusion coefficient of the particle as it moves parallel to the wall
$D_{\perp}$ - Reduced diffusion coefficient of the particle as it moves perpendicular to the wall

The exact analytical solution for the correction factor is complicated and is available for only special cases [44]. Hence, approximate solutions are used. These solutions are derived using the "method of reflections" [45]. These solutions are expressed as a power series of $\frac{a}{z}$, where a is the particle radius and z is distance from the centre of the sphere to the wall boundary.

$$\lambda_{\perp}^{-1} = \frac{D_{\perp}}{D_{||}} \cong 1 - \frac{9}{8}(\frac{a}{z}) + \frac{1}{2}(\frac{a}{z})^3 + O(\frac{a}{z})^4 \tag{4.13}$$

$$\lambda_{||}^{-1} = \frac{D_{\perp}}{D_{||}} \cong 1 - \frac{9}{16}(\frac{a}{z}) + \frac{1}{8}(\frac{a}{z})^3 - \frac{45}{256}(\frac{a}{z})^4 - \frac{1}{16}(\frac{a}{z})^5 + O(\frac{a}{z})^6 \tag{4.14}$$

Equations 4.13 and 4.14 represent higher order approximations. When $\frac{z}{a} \geq 1.6$, first order approximations can be used [41].

$$\lambda_{\perp}^{-1} = \frac{D_{\perp}}{D_{||}} \cong 1 - \frac{9}{8}(\frac{a}{z}) + O(\frac{a}{z})^3 \tag{4.15}$$

$$\lambda_{||}^{-1} = \frac{D_{\perp}}{D_{||}} \cong 1 - \frac{9}{16}(\frac{a}{z}) + O(\frac{a}{z})^3 \tag{4.16}$$

Above equations 4.13, 4.14, 4.15, 4.16 are valid when the particle is experiencing drag due to the presence of a single wall. But, when the particle is constrained to move between two walls, the

simplest analytical technique assumes it is reasonable to superimpose the effect of both the walls on the particle independently. Therefore,

$$f^{two} = F_{bulk}\lambda^{two} \cong F_{bulk} + F_{bulk}(\lambda^{one}_{wall1} - 1) + F_{bulk}(\lambda^{one}_{wall2} - 1) = F_{bulk}(\lambda^{one}_{wall1} + \lambda^{one}_{wall2} - 1) \tag{4.17}$$

where,
f^{two} - Total force on the sphere experiencing drag due to 2 walls
F_{bulk} - Force experienced by the particle far away from the wall
λ^{two} - 2 wall correction factor
λ^{one}_{wall1} - Single wall correction factor
λ^{one}_{wall2} - Single wall correction factor

$$\lambda^{two} \cong \lambda^{one}_{wall1} + \lambda^{one}_{wall2} - 1 \tag{4.18}$$

Therefore, the correction factor can be expressed as

$$\lambda^{two} = \lambda^{one}(z) + \lambda^{one}(d - z) - 1 \tag{4.19}$$

where,
d - Distance between the 2 walls

$$(\lambda^{two}_{||})^{-1} = \frac{D_{\perp}}{D_{Bulk}} \cong 1 - \frac{9}{16}[\frac{a}{z} + \frac{a}{d-z}] + O(\frac{1}{\frac{z}{a}})^2 \tag{4.20}$$

$$(\lambda^{two}_{\perp})^{-1} = \frac{D_{\perp}}{D_{Bulk}} \cong 1 - \frac{9}{8}[\frac{a}{z} + \frac{a}{d-z}] + O(\frac{1}{\frac{z}{a}})^2 \tag{4.21}$$

The theoretical estimate of the force experienced by a colloidal particle (a = 1.337 μm) as it moves parallel and normal to the wall is given in figure 4.4 and 4.5 respectively. The plot shows the force against the ratio of distance moved by the particle towards the wall (z) to the particle radius (a).

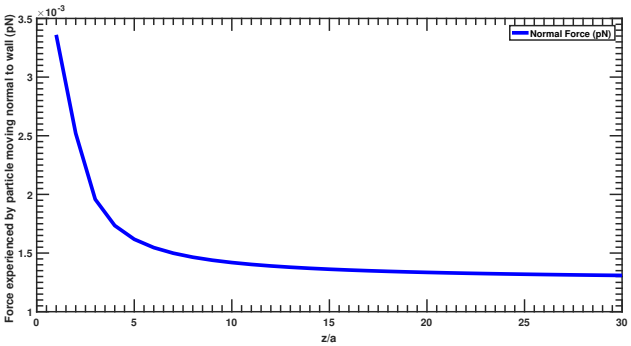

Figure 4.4: Drag force experienced by the particle as it moves normal to the wall

4.2. EXPERIMENT

4.2.1. SYSTEM DESCRIPTION

The system consists of a Zeiss Axio Observer D1 semi-motorized microscope with a diode pumped solid-state IR Nd:YAG (Laser Quantum Ventus 1064-3000) laser attached for optical trapping (wavelength = 1064 nm, power = 3W continuous wave). A 1.4 mega-pixel Axio ICc1 camera is attached to the left port of the microscope. A 0.63X camera adapter is used to connect the camera to the microscope. Tables 4.1 and 4.2 tabulate the microtweezer system and the IR laser specifications. Figure 4.6 represents the image of the tweezer apparatus

4.2.2. CALIBRATION

The microfluidic device is carefully filled with the experimental mixture (procedure described in section 3.2.3) using a 1 mL syringe. The microscope is started and the objective lens is covered

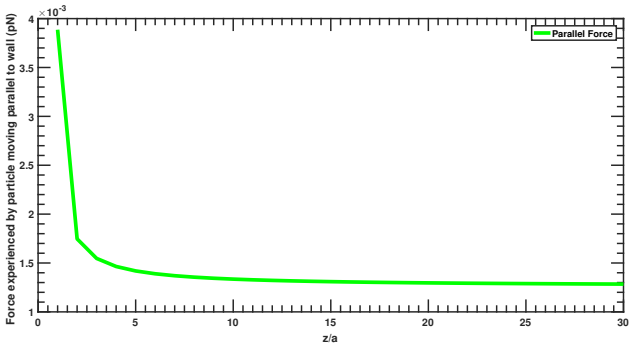

Figure 4.5: Drag force experienced by the particle as it moves parallel to the wall

(a) Zeiss Microscope

(b) PALM Microtweezer

Figure 4.6: Optical Tweezer apparatus

with the microscope immersion oil, Immersol^{TM}W (2010) . The device is placed on the stage and the channel is focused to locate the post positions and the particles. The inlet and the outlet ports are sealed with scotch tape to minimize drift. It is ensured that there was minimal visible flow of the liquid through the channel. The first step towards performing the depletion experiment is the system calibration. In order to calibrate the system, a fluorescent polystyrene bead is trapped and following parameters are provided to the system as input:-

1. Viscosity of the medium
2. Size of the particle
3. Force applied on the particle

The viscosity of the sample was measured, using the AR-G2 rheometer with couette geometry at 25 °C, to be 2 cP for the sample with the depletant and 1 cP for sample without depletant. The mean size of the colloidal particle is 1.337 μm with a coefficient of variance equal to 3 % (as per the maufacturer's specification). The DLS revealed the mean radius of gyration of the dextran to be 20 nm with a polydispersity index of 0.3. An image is taken, in the Transmitted Light (TL) mode, to capture the starting conditions. The viewing mode is switched to the Reflected Light (RL) mode and the calibration is started. The output of the calibration is the trap stiffness (k_x and k_y) along x and y direction. For an isotropic spherical bead, one would intuitively expect the trap stiffness along x and y directions to be the same. Multiple calibrations are performed to obtain the most precise values of trap stiffness with minimal uncertainty.

4.2.3. Depletion Experiment

During the depletion experiment, a particle is optically trapped and brought at a distance of approximately 30 μm from the post. Before starting the experiment, a reference position is automatically calculated by the system. The reference position is of vital importance because the deflection

Table 4.1: Specification of PALM MicroTweezer system

Tweezers	PALM MicroTweezers
Microscope	Axio Observer D1 semi motorized microscope
Objectives	Apochromat 63x/1.20W Korr UV VIS IR Plan- Apochromat 100x/1.40 oil EC Plan- Neofluor 10x/0.3 M27
Fluorescence	HXP 120W mercury short arc reflector lamp Mean life: 2000h
Whitefield	HAL100 with quartz collector
Stage	PALM Stage II motorized stage
Camera	Axio ICc1(1338 × 1038 @15 fps) 8 bit Camera Adapter 60N-C 2/3" 0.63x

Table 4.2: Specifications of the IR laser

Laser	Laser Quantum Ventus 1064-3000
Laser Class	1M, Enclosed Class 4 laser
Built year	2014
Wavelength	1064 nm (IR)
Max beam power	3 W

experienced by the particle is calculated based on this reference position. Following parameters are provided to the system as input:-

1. Direction of movement of the trapped particle
2. Velocity of the particle

Once the experiment is started, the trapped particle is moved automatically at the desired velocity toward the post. The experiment resulted in a graph and a spreadsheet. The spreadsheet tabulated the position (center of mass of the particle in X and Y direction), deflection experienced by the particle and force experienced by the particle in X and Y directions. The graph plotted the force experienced by the particle and the deflection from its reference position against time. A measurement is made without the addition of the depletant as a control measurement under the same optical and chemical conditions to determine any background interaction forces.

Precautions

Following precautions must be taken when depletion experiments are performed using optical tweezers.

1. Switch off the TL/RL mode and turn off the laser when it is not needed to avoid unnecessary heating of the liquid.
2. Images, before starting the experiment (to capture initial conditions) and once the experiment is completed (to capture the final conditions), must be taken in the TL mode for analysis. The boundary of the hard posts were visible in the RL mode and hence the post processing of the images containing interaction with hard posts was convenient. However, the boundary of the soft posts were not visible in the RL mode and therefore taking images before and after the experiment allows identifying the post positions.
3. Calibration must be performed multiple times at different locations and the calibration which results in the most precise values of trap stiffness should be used.
4. It must be ensured that there are no bubbles inside the channel once it is filled. The motion of the beads is significantly affected in the vicinity of a bubble.

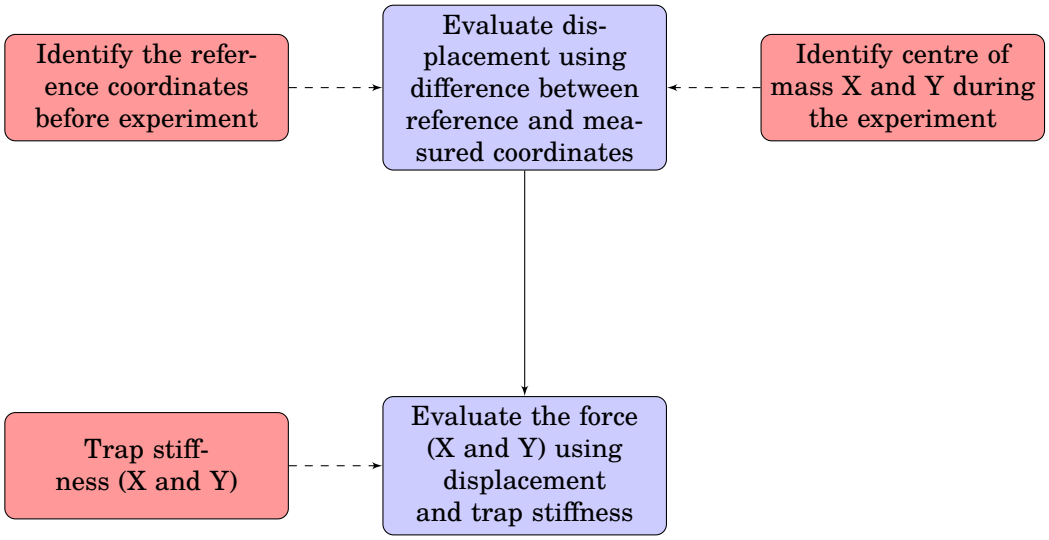

Figure 4.7: Flow scheme: Calculation of force experienced by the particle

Table 4.3: Error analysis during calibration and experiment

% Error in measured viscosity	4%
% Error in size	3%
% Error in velocity	0.1%
% Error in measured displacement (during calibration)	47 %
% Error in measured trap stiffness (during calibration)	48 %
% Error in measured force (during experiment)	48 %

4.3. Results and Discussion

4.3.1. Uncertainty in the measurement of force and trap stiffness

The uncertainty in the measurement of the force and the trap stiffness is very high (≈ 40 - 50 %) compared to the uncertainty observed in the literature (≈ 10%) [34] using similar apparatus. Based on the flow scheme shown in figure 4.7, it is clear that the uncertainty associated with particle displacement and trap stiffness is propagated into the measured force.

It was hypothesized that the uncertainty in the measured values of trap stiffness during calibration can be reduced by moving the particle over a range of velocities (80 μm/s to 160 μm/s). However, it was found that irrespective of the velocity, the uncertainty in trap stiffness remained high. Table 4.3 tabulates the error associated with the measurement of different parameters.

4.3.2. Particles irreversibly stuck to the post

The previous work [4] hypothesized that the incomplete cross-linking of the PEGDA hydrogel resulted in dangling free chains. It was proposed that these free chains were responsible for interacting with the PS particles and binding them irreversibly to the post. In this project, the PEGDA hydrogels were cured under the UV light for a period of 1.5 hours to ensure complete cross-linking.

But, during the experiments when the particle was moved to the post boundary, it was observed that the particle stuck to the post. Attempts were made to remove the particle from the post using the tweezer but the particle could not be removed.

Such irreversible binding to the post was seen with both the, hard and soft, hydrogel posts. It prevented the calculation of the escape time since the energy-potential curve described only the binding of the particle to the post but no reversible unbinding. Figure 4.8 shows the particles stuck to the hard post.

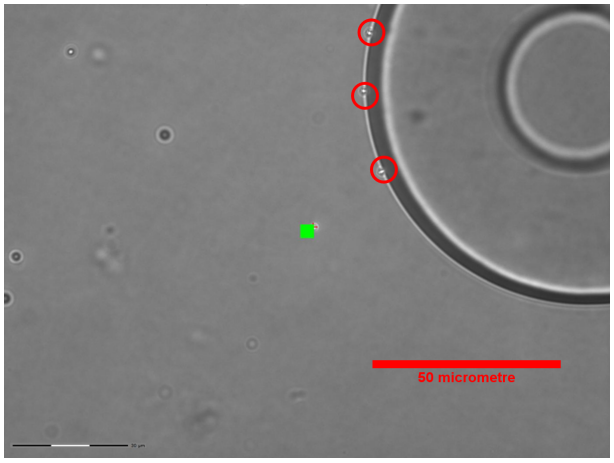

Figure 4.8: Particles irreversibly stuck to the hard post

4.3.3. Optical trapping of 2 particles simultaneously

The optical laser has a tendency to attract any particle in close proximity to the beam waist. During the initial experiments, the volume fraction of the colloidal particles in the experimental mixture was of the order of 10^{-5}.

But, when experiments were performed it was observed that this volume fraction was too high to conveniently perform depletion and control experiment. This is because the laser trapping a colloidal particles tended to attract another particle. It is easy to identify when a trap attracts more than 1 particle because the intensity of particle image suddenly increases. Figure 4.9 shows the increase in the intensity of the particle image when more than one particle is trapped by the laser. All experimental and calibration results based on two trapped particles were discarded. This issue was solved by diluting the colloidal particle suspension to a volume fraction of order of 10^{-7}.

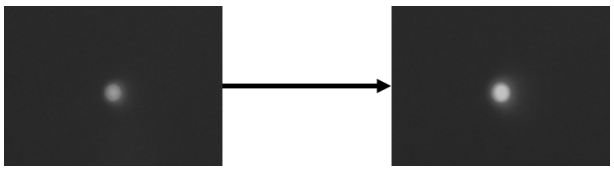

Figure 4.9: Two particle trapped together by the laser beam

4.3.4. Force-Displacement curve: Particle not moving

During some control and depletion experiments, it was observed that the trapped particle did not move from its original position. But, the force-displacement curve generated by the system showed the force experienced by the particle as it moved towards the post. Even though, based on the initial (before the experiment) and final image (after the experiment) of the particle, it was clearly visible that the particle was still at its original position.

It was initially thought that perhaps the trapped particle was stuck to the bottom wall of the channel. However, when the trap was switched off the particle moved away from its original position through Brownian motion. This proved that the particle was not stuck to the channel wall.

A common property under such situation was that the particle experienced a qualitatively increasing force as it moves towards the post and the magnitude of the force was 2 ($\pm$ 50%) pN. These results were assumed to be due to computer artifacts and were discarded from analysis. Figure 4.10 displays the force-displacement curve of a trapped particle not undergoing any motion.

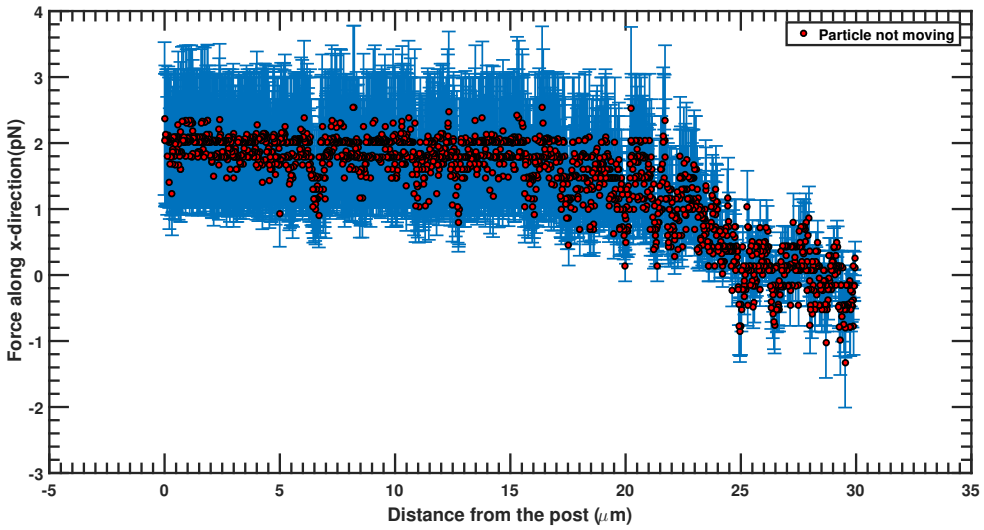

Figure 4.10: Force-Displacement curve for particles not moving

4.3.5. Distorted image of the particle

During the depletion experiments, it was commonly observed that the image of the trapped particle in the vicinity of the post was highly distorted. This distortion can be attributed to 3-D nature of the microfluidic system and therefore the force experienced by the particle along y- and z-directions due to the depletants. It is very important to remember that the basis of the force calculation, as described in the flow scheme 4.7, is the precise estimation of the centre of mass of the particle image as it moves towards the post. This estimation is based on the analysis of the particle image. If the image of the particle is distorted, as shown in 4.11, the estimated centre of mass may not be accurate. Consequently, the calculation of displacement and force will not be correct. Experiments with highly distorted image of the particles near the post were not considered for analysis.

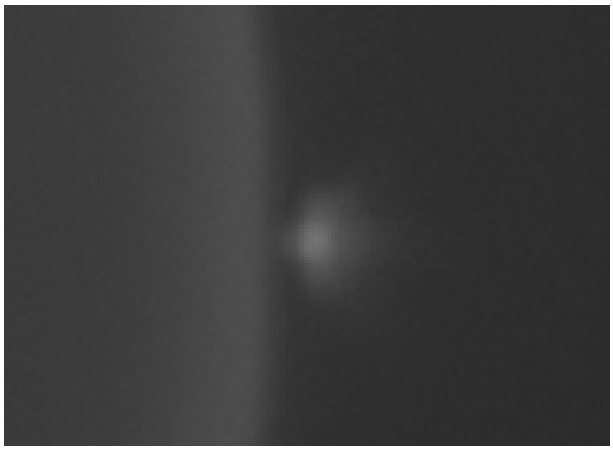

Figure 4.11: Distorted image of particle as it moves closer to the post during depletion interaction

4.3.6. Force experienced by the particle as it moves towards the post

During the control experiment, it was expected that as the particle moves closer the hydrogel post it would not experience any force near the post. This is because the experimental mixture contained only the diluted colloidal particles and the NaCl solution (to screen electrostatic interactions). However, it was observed that the particle experienced a force that qualitatively increased as it moved near the post. Since, there were no depletants in the experimental mixture, no interaction between the trapped colloidal particle and other suspended particles, it was hypothesized that this

force was due to the additional drag experienced by the particle due to its proximity with the bottom wall of the microfluidic channel (parallel to the particle motion) and increasing proximity with the post (normal to the particle motion).

In order to confirm this hypothesis, the position of the particle from the bottom of channel was determined using 4.9 and 4.14. The Stokes drag correction factor ($\lambda_{||}$) in Equation 4.14 is expressed as a ratio of $\frac{F_{||}}{F_{Bulk}}$ using equation 4.9. The resulting expression can be treated as a polynomial equation of the form

$$ax^5 + bx^4 + cx^3 + dx^2 + ex + f = 0 \tag{4.22}$$

This polynomial equation can then be solved to obtain its roots using MATLAB. The roots of the equation are the ratio of particle radius to the distance from the bottom wall ($\frac{a}{z}$). Since we already know the particle radius, the distance form the wall can be estimated.

This method is valid when the particle is at a distance of $\approx 20\mu$m from the post. At this distance ($\frac{z}{a} \approx 30$), the drag due to the post (normal to the direction of particle motion) is negligible [41].

The estimated height of the particle was 0.6 μm with a 95% confidence interval of 0.3 μm. This confirms that the particle experiences wall effects due to the bottom wall.

A quantitative comparison of the effect of drag, due to the motion of particle parallel to the wall and normal to the wall, theoretically (figures 4.4 and 4.5) with the experimental values, as shown in figure 4.12 and 4.13, suggests that the force experienced by the particle is greater than the predicted value. Hence, it is hypothesized that the effect of the corner (point of contact of the post and the bottom wall) also has an impact on the motion of the particle and must be estimated. Finally, based on the figures 4.14 and 4.15, a qualitative comparison of the force experienced by the particle as it moves closer to the post during the depletion experiment with force experienced by the particle during the control experiment suggests that near the post, force experienced by the particle increases. This can be considered as a proof of the existence of an interactive force between the colloidal particle and hydrogel post. Note that in figures 4.12, 4.14, 4.13 and 4.15, point zero on the x-axis denotes the point at which the surface to surface separation between the colloidal particle and the hydrogel post is zero.

However, it is difficult to establish if the force experienced by the particle is the depletion force because, for the given size of colloidal particle (ϕ = 1.337 μm) and the depletant (R_g = 20 nm), the depletion force must be of the order of 1 pN. But, the measured force is of the order of 10 pN.

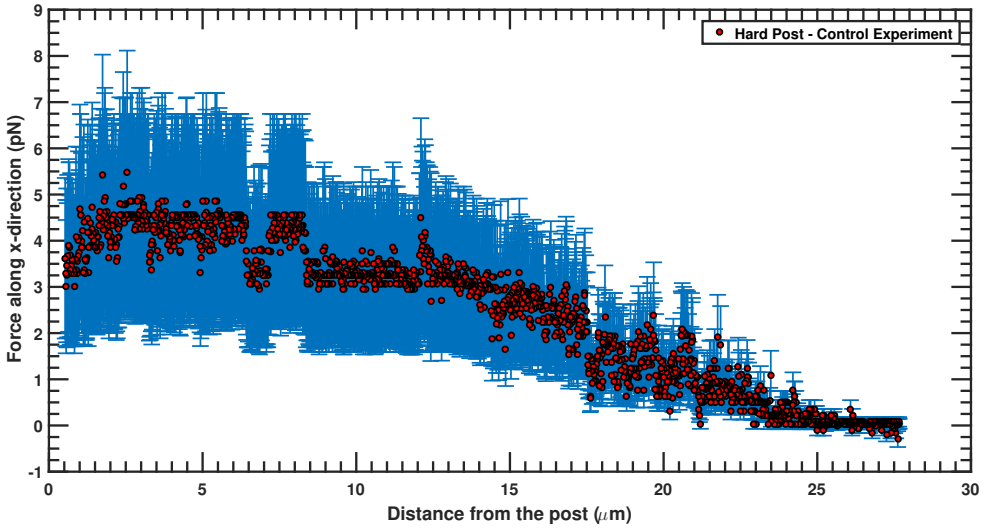

Figure 4.12: Force-Displacement curve: Control experiment for hard post

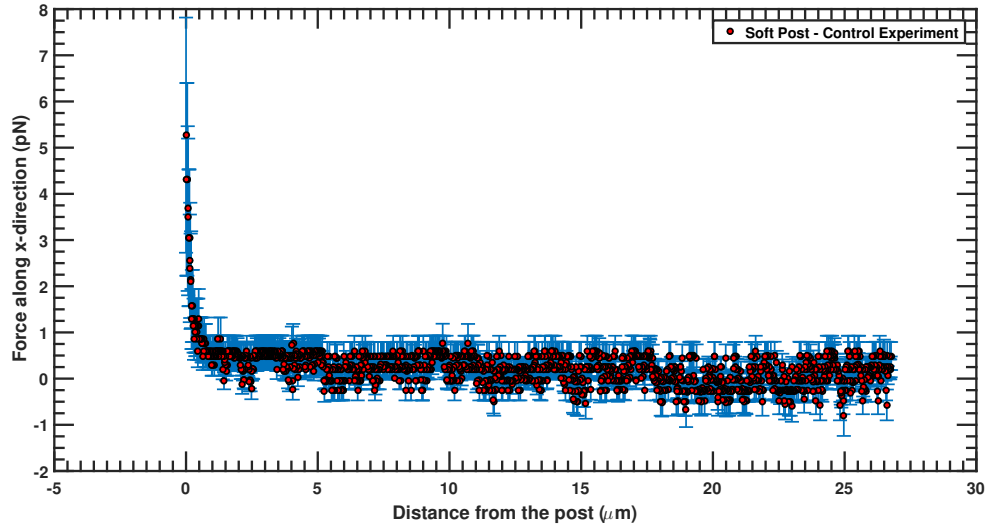

Figure 4.13: Force-Displacement curve: Control experiment for soft post

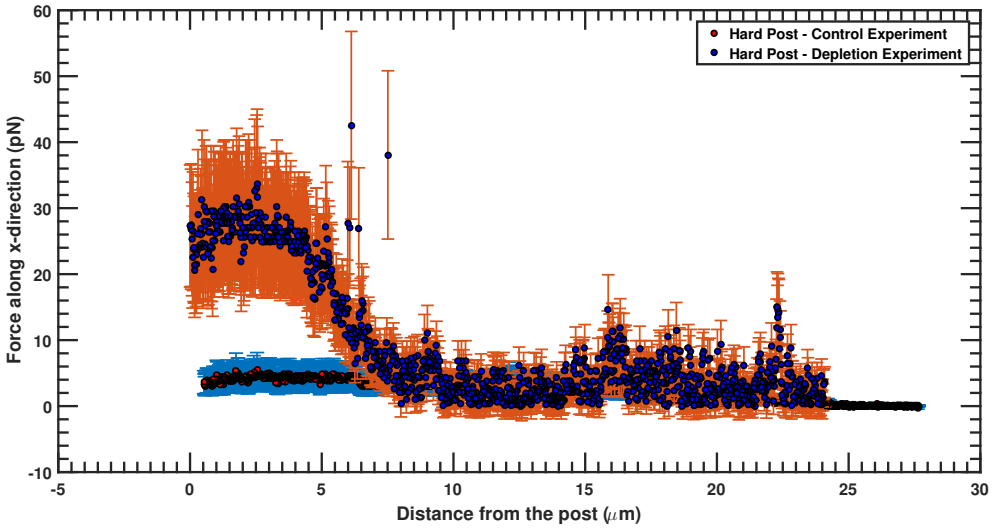

Figure 4.14: Force-Displacement curve: Comparison of control experiment and depletion experiment for hard post

4.4. Summary

1. The uncertainty associated with the trap stiffness and consequently the measured force is high. This uncertainty did not reduce when the particle was calibrated over a range of velocities.

2. The colloidal particles irreversibly bind to the hydrogel post. This irreversible binding is observed in spite of curing the hydrogel under UV light for 1.5 hours.

3. The adequate concentration of colloidal particle in the experimental mixture should be of the order of 10^{-7}. At this concentration, it is less probable to trap more than one particle. Experiments with more than one particle in the trap were discarded from analysis.

4. During some control experiments, it was observed that the particle did not move from its initial position (based on the initial and final images before and after the experiment respectively). But, the system generated a force vs displacement curve showing a force roughly 2 pN. These results were discarded from the analysis.

5. During depletion experiments, particle image near the post can become highly distorted. This

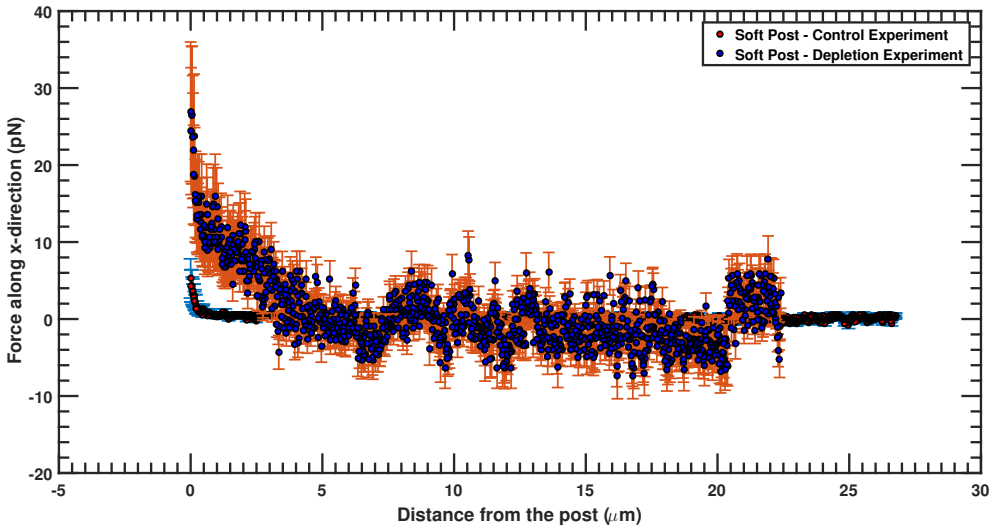

Figure 4.15: Force-Displacement curve: Comparison of control experiment and depletion experiment for soft post

distortion may result in incorrect estimation of the particle position. Experiments containing distorted image of the particle were discarded from analysis.

6. A qualitative increase in the force experienced by the particle is observed during the control experiment. This increase is attributed to the drag force due to the wall.

7. A quantitative comparison of depletion and control experiment reveal that the force experienced by the particle in the proximity to the post during depletion experiment is greater than the force experienced by the particle during the control experiment.

5
Conclusions & Recommendations

In this project, microscopic colloidal particles (ϕ 0.22 μm, ϕ 1.337 μm, ϕ 1.89 μm) were tracked, using the digital video microscopy technique, to estimate the bulk mechanical property of the particles in the suspended medium, i.e. diffusion coefficient of the colloidal particles in the aqueous medium. The errors associated with the tracking of particles, such as the drift flow in the sample, static error due to the experimental set-up, were quantified and corrected for when the particle trajectories were analyzed. The diffusion coefficient was estimated using the slope of the linear fit on the MSD against lag time curve. The propagation of error, due to curve fitting and the statistical uncertainty due to loss of displacements with increasing lag time, was considered and used for calculating the uncertainty associated with the estimated diffusion coefficient.
Based on the previous work [4], it was proposed that the incomplete cross-linking of the hydrogel (presence of dangling chains) was responsible for the colloidal particles to irreversibly attach to the post. It was hypothesized that longer exposure to the UV light will result in complete cross-linking and eliminate any dangling free chains. This should prevent particles from irreversibly attach to the post. Hence, in this project, hydrogel posts in water were cured for a period of 1.5 hours under UV light. It was inferred that the cross-linking density increased with increased exposure time based on the observation that the boundary of the hydrogel posts became more opaque upon curing. However, during the depletion experiments, using both digital video microscopy and the optical tweezers, it was observed that the colloidal particles irreversibly stick to the cured PEGDA post. Hence, it is recommended that the UV cross-linking characteristics of PEGDA hydrogels must be carefully studied and rheological tests should be performed to determine how the gel fraction of the hydrogel changes with increased exposure to UV light. Furthermore, to make the results of this study more reliable, it is recommended to analyze the shape of the hydrogel posts along the height of the channel to make sure that the posts are cylindrical throughout and not conical due to incomplete cross-linking.
The estimation of the escape time using simple particle tracking using video microscopy was rejected based on the poor statistics [4]. It was proposed that the optical tweezers offered a much better environment where particles could be trapped in direction normal to the hydrogel post (z-direction) and moved closer to the post in a controlled manner to reliably generate the energy-potential well and consequently calculate escape time precisely. Optical trapping, using PALM microtweezers, constrains the particle motion in z-direction and permits the user to displace the particle towards the post (+/- x-direction) in controlled manner. The apparatus provided the force (F_x,F_y) experienced by the particle, as the output, as the particle moved closer to the post. While this technique was more advantageous than the former method, the apparatus suffered from certain limitations:-

1. It is not possible to identify the location of particle along z-direction. This means that the distance of the particle from the top and bottom boundary of the microfluidic channel is unknown. This has important consequences. It is desired to trap the particle at a distance roughly 10 to 15 particle diameter away from the bottom to avoid wall effects.

2. The uncertainty associated with the trap stiffness is high ($\approx$ 48-52%). It was hypothesized that if particle was moved at lower velocities during calibration then the tarp stiffness light improve but when particle was moved at a range of velocities (from $\approx 80\mu$m/s to 160μm/s), no change was observed in the uncertainty associated with the trap stiffness. It is hypothesized that this uncertainty is because the system is calibrated using the Stokes law without faxen correction. The calibration can be performed using the Faxen correction however, this

requires informing the Microtweezer system about the position corresponding to the bottom of the channel. Since, system is not equipped to identify the z-position, the calibration can not be improved.

Efforts were made to determine the particle location (along the z-direction) by using the force output and the approximate solutions [41] describing the reduction in diffusion coefficient as the particle experiences additional drag due to the wall. The estimated value of z was roughly 0.6 μm with an uncertainty of 0.3 μm. This proved that the particle experienced additional drag due to the wall. This also explained qualitatively the increasing trend in the force experienced by the particle in x-y direction as it moves closer to the post during the control experiments. The measured forces in the control experiment were hypothesized to have originated due to the additional drag from the bottom channel wall and due to the hydrogel post as the particle comes closer to the post. Quantitatively, the measured force values (in x-y direction) did not match with the predicted theoretical values. The measured values were greater than the predicted value and it is hypothesized that the difference might be explained by the effect of the corner (where the hydrogel post and the bottom microfluidic wall connect). Hence, it is recommended that the effect of the corner on the particle drag should be predicted based on simulations using COMSOL.
The uncertainty associated with trap stiffness might be reduced by correcting for wall effects during calibration. But, this would require upgrading the existing microtweezer apparatus.
One has to remember that the system calculates the force values based on image analysis. Therefore, it is recommended that the measured force values are corrected for the thermal noise due to the camera.

6

Acknowledgement

I would like to express my gratitude to, first and foremost, my supervisor Burak Eral for his positive attitude, optimism and his faith in my abilities. Thank you for giving me the opportunity to work on your project and for pushing me to deliver to the best of my abilities.

I would like to thank, Rumen Georgiev, for teaching me how to use the microscope, how to prepare micrifluidic channels, for listening to my doubts and taking out time from his schedule to solve them.

I would like to thank, Jasper Landman, for helping me understand the idea and inspiration behind this project and for taking out time to listen to my results.

I would like to thank, Anne Weijkamp, for her work on the same project last year and for her report that helped me create a base for my understanding of the topic.

I would like to thank, Sara Toscano, for allowing to me observe how to prepare the channels for my experiments and for helping me if I got stuck while preparing the hydrogel posts on the microscope.

I would like to thank, Mehul Jain, for helping me perform DLS measurements at Applied Sciences.

I would like to thank, Ben Norder, from the ASM group to help me determine the viscosity of my samples.

I would like to thank, Luigi Sasso, from the PME group to provide me with the colloidal particle suspension that I could use for all my experiments.

I would like to thank Aswin Muralidharan and Pouyan Boukany for welcoming me into their lab and teaching me how to use optical tweezers. I would like to thank Aswin for taking out time from his busy schedule to solve my doubts.

I would like to thank Daniel Irimia for helping me set up the Zeiss microscope in the METH lab. This microscope will be useful for all the students who will work in the lab in future.

I would like to thank all my committee members Jan Van Esch and Othon Moultos for taking out time from their busy schedule to read my thesis and participate in my defence.

I express my gratitude towards all my fellow colleagues and employees at Process and Energy to provide an encouraging and friendly environment and for extending help whenever solicited.

Finally, I would like to thank my parents and my lovely sister for their strength and support when I doubted myself.

The success of this thesis is especially owed to my mother who has been and will forever be a source of inspiration for me.

At the end, I would like to congratulate all my friends and say “WE DID IT!”

working of optical tweezers.png working of optical tweezers.png Images/Images_model/Images_tweezer/

A

Deriving the expression for overlap volume

This derivation is based on the content available in [13].

The interaction area is the circular area of the cap (A) of the sphere defined by overlap of the depletion layers. This is integrated as we move the sphere closer to the wall. The overlap distance is $2R_g - H$. Overlap volume is a mathematical consequence of integrating the interaction area with the separation distance. The area of circle is given by

$$A = \pi m^2 \tag{A.1}$$

where,
A - Area of circle
m - Radius of circle
Therefore,

$$m^2 = 2ah - h^2 \tag{A.2}$$

$$\int_{h=0}^{h=2R_g-H} \pi(2(a+R_g)h - h^2)dh \tag{A.3}$$

Integrating,

$$\pi[2(a+R_g)\frac{h^2}{2} - \frac{h^3}{3}] \tag{A.4}$$

Applying the limits h=0 and $h = 2R_g - H$

$$\pi[2(a+R_g)\frac{(2R_g-H)^2}{2} - \frac{(2R_g-H)^3}{3}]\pi(2R_g-H)[(a+R_g) - \frac{(2R_g-H)}{3}] \tag{A.5}$$

So, finally

$$V_{overlap} = \pi(2R_g-H)^2[a + \frac{H}{3} + \frac{R_g}{3}] \tag{A.6}$$

B

Comparing the depletion interaction between sphere-sphere and sphere-plate

This derivation is based on the content available in [13].

At low concentration, the net interaction force between 2 colloidal particles immersed in a solution of non-adsorbing macromolecules will be given by

Case 1: 2 spherical particles of radius R, separated by gap width h, immersed in a solution of hard spherical macromolecules of radius a. Each isolated particle excludes a spherical volume of radius (a+R) from the macromolecules. When the particles approach sufficiently close however, these 2 excluded volumes overlap by the volume of the shaded region and therefore the total excluded volume of the system decreases by this amount

$$V_{Excluded} = V_{TotalExcluded} - V_{part-part}^{overlap} \tag{B.1}$$

So,

$$F = -K_B T \rho_\infty \frac{\partial V_{TotalExcluded}}{\partial V_{part-part}^{overlap}} \tag{B.2}$$

$$= KT\rho_\infty \frac{\partial V_{part-part}^{overlap}}{\partial h} \tag{B.3}$$

Th estimated overlap volume for 2 spherical particles is given by

$$V_{part-part}^{overlap} = \frac{2\pi}{3}(a - \frac{h}{2})^2(3R + 2a + \frac{h}{2}) \quad for \quad h < 2a \tag{B.4}$$

$$= 0 \quad for \quad h \geq 2a \tag{B.5}$$

Substituting C.9 in C.8

$$F = K_B T \rho_\infty \frac{\partial \frac{2\pi}{3}(a^2 + \frac{h^2}{4} - ah)(3R + 2a + \frac{h}{2})}{\partial h}$$

$$= \frac{2\pi K_B T \rho_\infty}{3}[(a^2 + \frac{h^2}{4} - ah)(\frac{1}{2}) + (3R + 2a + \frac{h}{2})(\frac{2h}{4} - a)]$$

$$= \frac{2\pi K_B T \rho_\infty}{3}[\frac{a^2}{2} + \frac{h^2}{8} - \frac{ah}{2} + \frac{6hR}{4} - 3aR + \frac{4ah}{4} - 2a^2 + \frac{h^2}{4} - \frac{ah}{2}]$$

$$= \frac{2\pi K_B T \rho_\infty}{3}[\frac{3h^2}{8} + \frac{3hR}{2} - 3aR - \frac{3a^2}{2}]$$

$$= \pi K_B T \rho_\infty [\frac{h^2}{4} + hR - 2aR - a^2]$$

$$= \pi K_B T \rho_\infty$$

$$aR[\frac{h^2}{4aR} + \frac{h}{a} - 2 - \frac{a}{R}]$$

So,

$$\frac{F_{part-part}}{\rho_\infty K_B T \pi a R} = -(2 + \frac{a}{R} - \frac{h}{a} - \frac{h^2}{4aR}) \quad for \quad 0 \le h < 2a \tag{B.6}$$

$$= 0 \quad for \quad h \ge 2a \tag{B.7}$$

Case 2: Depletion interaction between a single particle and a flat plate The depletion force will be given by

$$F_{part-plate} = K_B T \rho_\infty \frac{\partial V^{overlap}_{part-plate}}{\partial h'} \tag{B.8}$$

where h' is the gap between the particle and the plate

$$V^{overlap}_{part-plate} = \frac{\pi}{3}(2a - h')^2(3R + a + h') \quad for \quad h' < 2a \tag{B.9}$$

$$= 0 \quad for \quad h \ge 2a \tag{B.10}$$

So,

$$F_{part-plate} = K_B T \rho_\infty \frac{\partial \frac{\pi}{3}(2a - h')^2(3R + a + h')}{\partial h} \tag{B.11}$$

$$= K_B T \rho_\infty \frac{\pi}{3}[(2a - h')^2 + (3R + a + h')2(2a - h')(-1)]$$

$$= \frac{\pi}{3}\rho_\infty K_B T[4a^2 + h'^2 - 4ah' - 2(3R + a + h')(2a - h')]$$

$$= \frac{\pi}{3}\rho_\infty K_B T[4a^2 + h'^2 - 4ah' + (3R + a + h')(-4a + 2h')]$$

$$= \frac{\pi}{3}\rho_\infty K_B T[4a^2 + h'^2 - 4ah' + 6Rh' - 12aR - 4a^2 + 2ah' - 4ah' + 2h'^2]$$

$$= \frac{\pi}{3}\rho_\infty K_B T[3h'^2 - 6ah' + 6Rh' - 12aR]$$

$$F_{part-plate} = \pi \rho_\infty K_B T[h'^2 - 2ah' + 2Rh' - 4aR] \tag{B.12}$$

$$F_{part-plate} = \pi \rho_\infty K_B T a R[\frac{h'^2}{aR} - \frac{2h'}{R} + \frac{2h'}{a} - 4] \tag{B.13}$$

$$F_{part-plate} = -(4 + \frac{2h'}{R} - \frac{2h'}{a} - \frac{h'^2}{aR}) \quad for \quad h' < 2a \tag{B.14}$$

$$= 0 for h' \ge 2a \tag{B.15}$$

This is approximately twice the particle-particle interaction for R >> a.

C

Deriving the expression for Escape time

This derivation is based on the lecture notes available at [46].

The Kramer's problem is estimation of the rate at which a brownian particle escapes from a potential well over a potential barrier. The solution to this problem has been proposed based on the theory of "First passage times". There are many situations where it is required to determine the average time τ needed by a particle, undergoing diffusion under the influence of a potential well, to reach and bind to a target.
Let us suppose that the motion of a set of 'n' random particles a = (a_1,a_2,...,a_n) is dictated by Langevin equation. In a single experiment, particles will follow a specific path $a(t)$ as they wander through a-space. The initial point a_0 starts at t = 0 in a volume Ω bounded by a surface $\partial\rho$.
The first passage time is the first time that a particle leaves volume Ω. Due to the noise, a particle can lead different paths even upon repeating experiments, therefore, leading to different first passage times. In this problem, we have to determine a distribution of first passage passage times and specifically the mean first passage time.
The Langevin equation states that

$$\frac{d}{dt}a(t) = V(a) + \Xi(t) \tag{C.1}$$

where,
$V(a)$ - Streaming term
$\Xi(t)$ - Noise
The corresponding Fokker-Planck equation is

$$\frac{\partial}{\partial t}P(a,t) = -\frac{\partial}{\partial t}\Big[V(a)P(a,t)\Big] + \frac{\partial}{\partial a}\Big[D\frac{\partial}{\partial a}P(a,t)\Big] \tag{C.2}$$

Let us focus on those paths that have not left volume ρ by time t, so we have to remove all paths that have crossed the bounding surface $\partial\rho$ before time t. This can be implemented by using an absorbing boundary condition on $\partial\Omega$. Therefore, we have following two conditions Initial condition at t=0

$$P(a,t) = \delta(a - a_0) \tag{C.3}$$

Absorbing condition on boundary $\partial\Omega$

$$P(a,t) = 0 \tag{C.4}$$

Let us use the Fokker-Planck operator L_{FP} to re-write C.1 in more convenient format

$$\frac{\partial P}{\partial t} = -L_{FP}P \tag{C.5}$$

where,

$$L_{FP} = \frac{\partial}{\partial a}V(a) - \frac{\partial}{\partial a}(D\frac{\partial}{\partial a}) \tag{C.6}$$

Due to the absorbing boundary condition, C.4, we can write

$$P(a, t \to \infty) = 0 \tag{C.7}$$

The probability that the brownian particle is still in volume Ω at time time t is given by $G(t)$

$$G(t) = \int_{\Omega} P(a,t)\,da \tag{C.8}$$

This equation C.8 is equal to the probability that the first passage time (τ) from a_0 to $\partial\Omega$ is larger than t

$$G(t) = P(\infty < \tau < t) = \int_{\tau=t}^{\tau=\infty} \rho(\tau)\,d\tau = -\int_{\tau=\infty}^{\tau=t} \rho(\tau)\,d\tau \tag{C.9}$$

where,
$\rho(\tau)$ - Probability density function for first passage time
Differentiating both sides of equation C.9 with respect to τ

$$-\frac{\partial G(t)}{\partial \tau} = \rho(\tau) \tag{C.10}$$

The mean first passage time is the first moment of τ

$$\langle \tau \rangle = \int_{\tau=0}^{\tau=\infty} \tau\rho(\tau)\,d\tau \tag{C.11}$$

Substituting the value of $\rho(\tau)$ from C.10 in C.11

$$\langle \tau \rangle = -\int_{\tau=0}^{\tau=\infty} \tau \frac{\partial G}{\partial \tau}\,d\tau \tag{C.12}$$

Applying integration by parts on C.12,

$$= -\int_{\tau=0}^{\tau=\infty} \tau \frac{\partial}{\partial \tau}\Big(\int_{\Omega} da P(a,t)\Big)d\tau = \int_{\tau=0}^{\tau=\infty} G(\tau)\,d\tau \tag{C.13}$$

Therefore,

$$\langle \tau \rangle = \int_{\tau=0}^{\tau=\infty} d\tau \int_{\Omega} P(a,\tau)\,da \tag{C.14}$$

Rewriting equation C.14,

$$\langle \tau \rangle = \int_{\Omega} \Big[\int_{\tau=0}^{\tau=\infty} P(a,\tau)\,d\tau\Big]\,da \tag{C.15}$$

Let $\int_{\tau=0}^{\tau=\infty} P(a,\tau)\,d\tau = g_1(a)$ So, the problem is of calculating $\langle \tau \rangle$ is now reduced to estimation of $g_1(a)$ So, in order to estimate the $g_1(a)$, we apply the Fokker-Planck operator, L, to both sides of expression defining $g_1(a)$. Therefore,

$$Lg_1(a) = \int LP(a,\tau)\,d\tau \tag{C.16}$$

We know that, $LP = \frac{\partial P}{\partial t}$, therefore,

$$Lg_1(a) = \int_{t=0}^{t=\infty} \frac{\partial P(a,t)}{\partial t}\,dt = P(a,t)|_{t=0}^{t=\infty} = P(a,\infty) - P(a,0) = -P(a,0) \tag{C.17}$$

The initial condition C.3 states that

$$P(a, t=0) = \delta(a - a_0) \tag{C.18}$$

Therefore,

$$Lg_1(a) = -P(a,0) = -\delta(a - a_0) \tag{C.19}$$

Assuming the force field to be conservative, which implies

$$F = -\frac{\partial U(x)}{\partial x} \tag{C.20}$$

we can re-define $g_1(a)$ using the Fokker-Planck operator

$$Lg_1(a) = D\Big[\frac{\partial^2 g_1}{\partial a^2} + \frac{1}{K_B T}\frac{\partial}{\partial a}(U'(a)g_1)\Big] \tag{C.21}$$

$$= D\Big[\frac{\partial^2 g_1}{\partial a^2} + \frac{U'(a)}{K_B T}\frac{\partial g_1}{\partial a} + g_1\frac{U"(a)}{K_B T}\Big]$$

$$= D\frac{\partial}{\partial a}\Big[\frac{\partial g_1}{\partial x} + \frac{U'(a)}{K_B T}g_1\Big]$$

$$= D\frac{\partial}{\partial x}\Big[\exp\big(-\frac{U(a)}{K_B T}\big)\frac{\partial}{\partial a}\Big(\exp(\frac{U(a)}{K_B T}g_1(a))\Big)\Big]$$

$$\Big\{= D\frac{\partial}{\partial a}\Big[\exp\big(-\frac{U(a)}{K_B T}\big)\Big\{\exp\big(\frac{U(a)}{K_B T}\big)\frac{\partial g}{\partial a} + \frac{g_1}{K_B T}\exp\big(\frac{U(a)}{K_B T}\big)\frac{\partial U}{\partial a})\Big\}\Big]$$

$$= D\frac{\partial}{\partial a}\Big[\frac{\partial g_1}{\partial a} + \frac{\partial U}{\partial a}(\frac{g_1(a)}{K_B T})\Big]\Big\}$$

So, now we have a relation

$$Lg_1(a) = D\frac{\partial}{\partial a}\Big[\exp(\frac{-U}{K_B T})\frac{\partial}{\partial a}\big(\exp(\frac{U}{K_B T})g_1\big)\Big] = -\delta(a)$$

$$\int\frac{\delta(a)}{D} = \exp\big(\frac{-U}{K_B T}\big)\frac{\partial}{\partial a}\Big(g_1\exp\big(\frac{U}{K_B T}\big)\Big)$$

$$-\int\Big(\exp(\frac{U}{K_B T})(\int\frac{\delta}{D})\Big) = g_1\exp\big(\frac{U}{K_B T}\big)$$

$$g_1 = \frac{-1}{D}\exp(\frac{-U}{K_B T})\int\exp\big(\frac{U}{K_B T}\big)\Big[\int\frac{\delta}{D}\Big]$$

The mean passage time is

$$\langle\tau\rangle = \int g_1(a)da \tag{C.22}$$

Introducing variables x, y, z for the boundary conditions

$$= -\frac{1}{D}\int_{x=-x_A}^{x=x_A}\Big[\exp\big(\frac{-U(x)}{K_B T}\big)\Big\{\int_{y=x}^{y=x_A}\exp\Big(\frac{U(y)}{K_B T}\Big)\Big[\int_{z=0}^{z=y}\delta(z)dz\Big]dy\Big\}dx\Big]$$

$$= -\frac{1}{2D}\int_{x=-x_A}^{x=x_A}\Big[\exp\big(\frac{-U(x)}{K_B T}\big)\Big\{\int_{y=x}^{y=x_A}\exp\Big(\frac{U(y)}{K_B T}\Big)dy\Big\}dx\Big]$$

$$= -\frac{1}{D}\int_{x=0}^{x=x_A}\Big[\exp\big(\frac{-U(x)}{K_B T}\big)\Big\{\int_{y=x}^{y=x_A}\exp\Big(\frac{U(y)}{K_B T}\Big)dy\Big\}dx\Big]$$

$$= \frac{1}{D}\int_{x=0}^{x=x_A}\Big[\exp\big(\frac{-U(x)}{K_B T}\big)\Big\{\int_{y=x_A}^{y=x}\exp\Big(\frac{U(y)}{K_B T}\Big)dy\Big\}dx\Big]$$

So, the mean escape time is

$$\langle\tau\rangle = \frac{1}{D}\int_{x=0}^{x=x_A}\Big[\exp\big(\frac{-U(x)}{K_B T}\big)\Big\{\int_{y=x_A}^{y=x}\exp\Big(\frac{U(y)}{K_B T}\Big)dy\Big\}dx\Big] \tag{C.23}$$

Bibliography

[1] A. W. Fenton, *Allostery: an illustrated definition for the 'second secret of life',* Trends in biochemical sciences **33**, 420 (2008).

[2] J. Monod, J.-P. Changeux, and F. Jacob, *Allosteric proteins and cellular control systems,* in *Selected Papers in Molecular Biology by Jacques Monod* (Elsevier, 1978) pp. 547–570.

[3] W. A. Eaton, E. R. Henry, J. Hofrichter, S. Bettati, C. Viappiani, and A. Mozzarelli, *Evolution of allosteric models for hemoglobin,* IUBMB life **59**, 586 (2007).

[4] A. Weijkamp, *Colloidal Allostery*, Master's thesis (2017).

[5] J. C. Crocker and D. G. Grier, *Methods of digital video microscopy for colloidal studies,* Journal of colloid and interface science **179**, 298 (1996).

[6] T. M. Squires and T. G. Mason, *Fluid mechanics of microrheology,* Annual review of fluid mechanics **42** (2010).

[7] E. M. Furst and T. M. Squires, *Microrheology*, 1st ed. (Oxford:Oxford University Press, 2017) pp. 135–198.

[8] T. Savin and P. S. Doyle, *Static and dynamic errors in particle tracking microrheology,* Biophysical journal **88**, 623 (2005).

[9] J. Perrin, *Brownian movement and molecular reality* (Courier Corporation, 2013).

[10] J. C. Crocker and B. D. Hoffman, *Multiple-particle tracking and two-point microrheology in cells,* Methods in cell biology **83**, 141 (2007).

[11] R. M. Mazo and Y. Peres, *Brownian motion* (Cambridge University Press, 2010).

[12] K. J. Beers, *Numerical methods for chemical engineering: applications in Matlab* (Cambridge University Press, 2006).

[13] H. N. Lekkerkerker and R. Tuinier, *Colloids and the depletion interaction*, Vol. 833 (Springer, 2011).

[14] J. M. Smith, *Introduction to chemical engineering thermodynamics,* (1950).

[15] M. Mravlak, *Depletion force,* University of Ljubljana , 3 (2008).

[16] A. Vrij, *Polymers at interfaces and the interactions in colloidal dispersions,* Pure and Applied Chemistry **48**, 471 (1976).

[17] H. d. Hek and A. Vrij, *Phase separation in non-aqueous dispersions containing polymer molecules and colloidal spheres,* Journal of Colloid and Interface Science **70**, 592 (1979).

[18] S. Asakura and F. Oosawa, *Interaction between particles suspended in solutions of macromolecules,* Journal of Polymer Science Part A: Polymer Chemistry **33**, 183 (1958).

[19] S. Asakura and F. Oosawa, *On interaction between two bodies immersed in a solution of macromolecules,* The Journal of Chemical Physics **22**, 1255 (1954).

[20] P. Malo de Molina, S. Lad, and M. E. Helgeson, *Heterogeneity and its influence on the properties of difunctional poly (ethylene glycol) hydrogels: Structure and mechanics,* Macromolecules **48**, 5402 (2015).

[21] M. A. Traore and B. Behkam, *A peg-da microfluidic device for chemotaxis studies,* Journal of Micromechanics and Microengineering **23**, 085014 (2013).

[22] B. V. Slaughter, S. S. Khurshid, O. Z. Fisher, A. Khademhosseini, and N. A. Peppas, *Hydrogels in regenerative medicine,* Advanced materials **21**, 3307 (2009).

[23] J. W. Hwang, S. M. Noh, B. Kim, and H. W. Jung, *Gelation and crosslinking characteristics of photopolymerized poly (ethylene glycol) hydrogels,* Journal of Applied Polymer Science **132** (2015).

[24] N. Sanabria-DeLong, A. J. Crosby, and G. N. Tew, *Photo-cross-linked pla-peo-pla hydrogels from self-assembled physical networks: mechanical properties and influence of assumed constitutive relationships,* Biomacromolecules **9**, 2784 (2008).

[25] R. W. Ogden, *Non-linear elastic deformations* (Courier Corporation, 1997).

[26] V. L. Popov, *Contact mechanics and friction* (Springer, 2010).

[27] K. K. Chawla and M. Meyers, *Mechanical behavior of materials* (Prentice Hall, 1999).

[28] K. Kegler, M. Salomo, and F. Kremer, *Forces of interaction between dna-grafted colloids: An optical tweezer measurement,* Physical review letters **98**, 058304 (2007).

[29] X. Wang, Z. Wang, and D. Sun, *Cell sorting with combined optical tweezers and microfluidic chip technologies,* in *Control Automation Robotics & Vision (ICARCV), 2010 11th International Conference on* (IEEE, 2010) pp. 201–206.

[30] R. J. Clarke, K. Högnason, M. Brimacombe, and E. Townes-Anderson, *Cone and rod cells have different target preferences in vitro as revealed by optical tweezers,* Molecular vision **14**, 706 (2008).

[31] A. L. Stout, *Detection and characterization of individual intermolecular bonds using optical tweezers,* Biophysical journal **80**, 2976 (2001).

[32] D. delToro and D. E. Smith, *Accurate measurement of force and displacement with optical tweezers using dna molecules as metrology standards,* Applied physics letters **104**, 143701 (2014).

[33] S. B. Smith, Y. Cui, and C. Bustamante, *Overstretching b-dna: the elastic response of individual double-stranded and single-stranded dna molecules,* Science **271**, 795 (1996).

[34] M. Salomo, K. Kroy, K. Kegler, C. Gutsche, M. Struhalla, J. Reinmuth, W. Skokov, C. Immisch, U. Hahn, and F. Kremer, *Binding of tmhu to single dsdna as observed by optical tweezers,* Journal of molecular biology **359**, 769 (2006).

[35] K.-h. Lin, J. C. Crocker, A. C. Zeri, and A. Yodh, *Colloidal interactions in suspensions of rods,* Physical review letters **87**, 088301 (2001).

[36] Y. Ohshima, H. Sakagami, K. Okumoto, A. Tokoyoda, T. Igarashi, K. Shintaku, S. Toride, H. Sekino, K. Kabuto, and I. Nishio, *Direct measurement of infinitesimal depletion force in a colloid-polymer mixture by laser radiation pressure,* Physical review letters **78**, 3963 (1997).

[37] R. Verma, J. C. Crocker, T. C. Lubensky, and A. Yodh, *Entropic colloidal interactions in concentrated dna solutions,* Physical review letters **81**, 4004 (1998).

[38] I. Titushkin and M. Cho, *Distinct membrane mechanical properties of human mesenchymal stem cells determined using laser optical tweezers,* Biophysical journal **90**, 2582 (2006).

[39] P. H. Jones, O. M. Maragò, and G. Volpe, *Optical tweezers: Principles and applications* (Cambridge University Press, 2015).

[40] M. Gögler, *Laser microtweezers get a grip on your cells,* (2012).

[41] B. Lin, J. Yu, and S. A. Rice, *Direct measurements of constrained brownian motion of an isolated sphere between two walls,* Physical Review E **62**, 3909 (2000).

[42] G. MacKay and S. Mason, *Approach of a solid sphere to a rigid plane interface,* Journal of Colloid Science **16**, 632 (1961).

[43] W. B. Russel, D. A. Saville, and W. R. Schowalter, *Colloidal dispersions* (Cambridge university press, 1989).

[44] P. Ganatos, R. Pfeffer, and S. Weinbaum, *A strong interaction theory for the creeping motion of a sphere between plane parallel boundaries. part 2. parallel motion,* Journal of Fluid Mechanics **99**, 755 (1980).

[45] J. Happel and H. Brenner, *Low Reynolds number hydrodynamics: with special applications to particulate media*, Vol. 1 (Springer Science & Business Media, 2012).

[46] L. Sjögren, *The kramers problem and first passage times.* (2012).

List of Tables

List of Figures

List of abbreviations

BF Bright Field. 22, 25, 26, 54

DI De-ionized. 10

DLS Dynamic Light Scattering. 32

EPI Epifluorescence microscopy. 4, 5, 25, 54

FITC Fluorescein isothiocyanate. 25, 26, 54

IR Infrared. 27, 31, 33, 53

M.W. Molecular Weight. 14

MSD mean squared displacement. 4, 7–11, 13, 40, 54

MSE Mean Squared Error. 9

NA numerical aperture. 27, 28

Nd:YAG Neodymium-doped yttrium aluminum garnet. 27, 31

PDMS polydimethylsiloxane. 20

PEG polyethyleneglycol. 16, 22

PEGDA Polyethyleneglycol diacrylate. 1, 14, 16–18, 21, 22, 25, 27, 34, 40

PI photoinitiator. 16

PS Polystyrene. 1, 2, 14, 34

RL Reflected Light. 32, 33

SNR Signal-to-Noise ratio. 5

TL Transmitted Light. 32, 33

TPM 3-(Trimethoxysilyl)propyl methacrylate. 21

UV Ultraviolet. 1, 2, 10, 22, 23, 25, 34, 38, 40

List of Symbols

$2a$	Contact diameter	
$2w$	Diameter of colloidal particles	$pixels$
α	Polarizability of light	
Δx	Particle displacement form reference position	
δ	Distance a particle can diffuse in the suspended medium	
δ	Phase angle	
$\Delta^2(\tau)$	Width (or variance) of fitted Gaussian distribution	
$\delta_0(\tau)$	Drift in the sample of particles due to bulk flow in particle tracking	
ϵ	Particle location correction	
η	Viscosity of the medium	
λ^{one}_{wall1}	Single wall correction factor	
λ^{two}	2 wall correction factor	
$\lambda_\perp$	Correction factor to the Stokes drag force as particle moves perpendicular to the wall	
λ_D	Screening length	
$\lambda_{\|\|}$	Correction factor to the Stokes drag force as particle moves parallel to the wall	
λ^{one}_{wall2}	Single wall correction factor	
$\mathbf{r_i}$	Position vector	
μ	micro	
ϕ	Diameter of sphere	
ϕ_0	Polymer concentration in hydrogel	
ϕ_{poly}	Volume fraction of macromolecule in depletion mixture	
τ	Time required by the particle to diffuse over a distance δ in the suspended medium	
ε	Ratio of penetration depth to the contact diameter	
ξ	Half-width of a pixel	
A	Area of contact	
b_0	Intercept	
b_1	Slope	
C_{equi}	Concentration of salt in bulk	
D	Diffusion coefficient of the particle	
d	Number of dimensions in the trajectory data	

d	Penetration depth
$D_{\perp}$	Reduced diffusion coefficient of the particle as it moves perpendicular to the wall
$D_{\|\|}$	Reduced diffusion coefficient of the particle as it moves parallel to the wall
E	Elastic modulus
E	Electric field
e	Charge on electron
$E()$	Expectation value
E	Tensile loss modulus
$E^{'}$	Tensile storage modulus
f^{two}	Total force on the sphere experiencing drag due to 2 walls
$F_{\perp}$	Drag force experienced by the particle as it moves perpendicular to the wall
$F_{\|\|}$	Drag force experienced by the particle as it moves parallel to the wall
F_{Bulk}	Drag force experienced by the particle as it moves far away from the wall
F_{bulk}	Force experienced by the particle far away from the wall
F_{rest}	Restoring force
F_{rest}	Restoring force
g	Faxen correction factor
G	Shear loss modulus
$G^{'}$	Shear storage modulus
G_0	Shear elastic modulus
h	surface to surface separation between colloidal particle and post
I	Intensity of light
$I(x,y)$	Intensity of particle image
I_w	Pixel value
k	Trap Stiffness
k	Trap stiffness
m_1	Radius of gyration of particle image
m_o	Integrated brightness
N	Number of particles
n_b	Number density of macromolecule is mixture
n_b^*	Number density of macromolecule is mixture at overlap concentration
N_{disp}	Number of displacments at a given lag time
P	Dipole moment in the sphere induced by the light
Q	Free energy of macromolecule

R	Radius of rigid sphere	
r	Radius of the particle	
R_g	Radius of gyration	
s	Standard deviation of the set	
t	Student t factor	
U	Energy produced by electric field	
U_m	Uncertainty of the mean	
V	Constant velocity of the particle	
$V_{Excluded}$	Excluded volume	
V_{free}	Free volume available to macromolecules	
V_O	Overlap volume	
V_{Total}	Total volume	
$w(x)$	Free energy of the macromolecule as a function of position x	
Z	Ionic charge	
m_0	Integrated brightness of particle image	
M	Molarity	mol/L